ON PARKING SOLUTIONS AROUND EUROPA

Martin Lara*, Ryan Russell†, Benjamin Villac†

The long-term stable trajectories around Europa, one of the Galilean moons of Jupiter, are analyzed for their potential applications in spacecraft trajectory design, such as end of mission disposal options, backup orbits, or intermediary targets for transfer trajectories. The phase space is analyzed via the computation of families of periodic orbits and the estimation of their associated stability domains using a Fast Lyapunov Indicator method. While the core analysis of the paper uses the circular restricted three body problem, a selected set of parking solutions is checked by integrating the corresponding initial conditions in an ephemeris model over several years.

INTRODUCTION

The design of space missions with close range analysis of potentially life harbouring celestial bodies are generally constrained by planetary protection measures. Such requirements directly result in constraints on lifetime and recovery margins to be taken into account in the design of the spacecraft trajectory. For example, non-impact conditions with a celestial body must not only be satisfied for the nominal trajectory under nominal hardware conditions, but must also encompass the evolution of the spacecraft in the event of mis-thrust or other propulsion system problems. In the worst case scenario, a complete loss of thrust during a maneuver may result in placing the spacecraft in unstable environment from which the nominal course of the mission may be difficult, or impossible, to recover.

Periodic or quasi-periodic stable trajectories can be used to achieve such goals as the natural dynamics do not lead a spacecraft into risky episodes. A missed maneuver opportunity starting from such stable trajectories will only require to wait a few periods before new opportunities can be found. Also, as these stable trajectories are indeed compounded into open regions of phase space, or stability islands, small perturbations along the trajectories will not lead the spacecraft to leave these regions. Thus transfers lying inside stability regions at all times present desirable robustness properties, though most likely, at the cost of larger fuel than transfers performed in unstable regions. The stable option, may nevertheless be an option for some legs of a long trajectory. Also, These islands of stable dynamics can be used as intermediary targets in transfer design problems to allow for longer mission lifetime and better recovery properties [1], as well as back-up options. These islands will thus be referred to as parking solutions.

While the stability of an orbiter close to Europa has been considered in several papers [2, 3, 4, 5, 6], the exploration of more distant stable regions has received much less attention, except for the case

*Commander, Ephemeris Department, Real Observatorio de la Armada, 11110 San Fernando, Spain. E-mail: mlara@roa.es

†Member of the engineering staff, Guidance, Navigation and Control section, Jet Propulsion Laboratory, California Institute of Technology, Mail Stop 301-140L, 4800 Oak Grove Drive, Pasadena, CA 91109-8099. E-mails: Ryan.Russell@jpl.nasa.gov and Benjamin.Villac@jpl.nasa.gov.

of distant retrograde orbits (DRO) [7, 8]. This paper aims at discussing and characterizing the main classes of the more distant parking solutions that exist around Europa.

The approach taken uses the circular restricted three-body problem (CRTBP) to model the underlying dynamics and aims at computing families of periodic orbits that bifurcate from the main planar families. This analysis is complemented by the computation of stability maps based on a Fast Lyapunov Indicator [9, 10] in order to estimate the extent of the stability regions that exist around the main stable periodic orbits. This grouping of families of trajectories allows us to evaluate the different sets of parking solutions on their robustness properties, as well as their physical configuration in position space.

After reviewing the basic dynamical notions of interest for this paper, the computation and relations among the different families of periodic orbits are considered. Finally, a discussion on the different classes of parking solutions and an evaluation of their robustness to perturbation in a more realistic model than the CRTBP is given.

DYNAMICAL BACKGROUND AND TOOLS

While the very long-term stability properties of some regions of phase space may differ substantially between a CRTBP and a more realistic model of the dynamics [11], the sets of trajectories of interest in this paper should be, by definition, robust with respect to small enough perturbations and thus continue to exist in the CRTBP. The choice of this model for our analysis has the advantage of resulting in faster numerical integration routines and represents an autonomous hamiltonian approximation to the dynamics (availability of an integral of motion) which simplifies the analysis in some cases. For the readers convenience, a quick review of the basic dynamics in this model is provided in appendix, while the topics more relevant for the remainder are reviewed in this section. References for this background can be found in [13, 12].

Mixed phase space

Besides the unavailability of closed form solutions for the CRTBP, many of the challenges in analyzing the CRTBP dynamics comes from the complexity of the orbit structure in phase space. While the set of trajectories of an integrable system is nicely foliated by invariant tori on which periodic and quasi-periodic orbits lie, the presence of perturbations, such as the presence of the secondary in the model considered, result in the destruction of some of these tori, leaving the place to a mixture of chaotic and regular motion. Chaotic motion associate with the idea of high sensitivity with respect to the initial conditions is the result of transversal intersection of hyperbolic manifolds of unstable periodic orbits, while regular motion is defined as the remaining set of stable periodic and quasi-periodic trajectories.

As the size of the third-body perturbation increases (e.g., a decrease in the Jacobi constant, C) chaotic motion tends to dominate the phase space, while the regular trajectories tend to clump themselves into open regions of phase space, referred to as stability islands, or regions. This is illustrated in Figure 1, which presents a Poincaré map [13] of the planar problem at a fixed Jacobi constant.

While the concept of stability region is less definite than that of chaotic or regular motion, it is of immediate practical interest. These regions are defined as sets of trajectory legs staying close together* for a given length of time (assumed to be large from a practical viewpoint, e.g. larger than 10 years), and thus capture the notion of practical stability needed for spacecraft applications. In the case when chaotic motion tends to dominate the phase space, the stability islands are well approximated by the numerical estimation† of the set of regular motion. The type of motion near

*Distance is here defined in terms of orbital nearness and not statewise distance. For example, two circular orbits differening only by a small difference in their semi-major axis are near in the orbital sense.

†And thus the resolution of the dynamics up to a finite resonance order

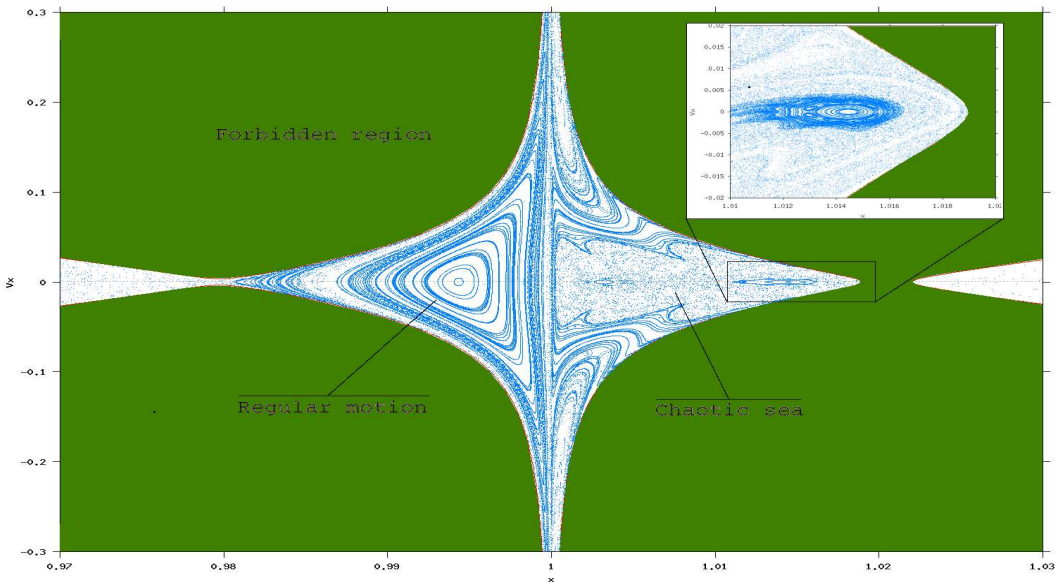

Figure 1: Example of a Poincaré map at fixed Jacobi constant ($C = 3.00363$) in the normalized Jupiter-Europa planar CRTBP ($\mu = 2.528 \times 10^{-5}$). The zoom window presents a more detailed view on a stability island immersed in the chaotic sea.

the boundary of such regions presents large variations in dynamical behavior, appearing as a sharp transition from regular to chaotic motion.

While Poincaré maps give a useful qualitative picture of stability islands in the planar problem, the investigation of these regions in the CRTBP requires the use of different dynamical tools. As Figure 1 suggests, the stability islands are associated with stable periodic orbits which form the backbone structure of these islands. Periodic orbits allow us also to investigate the bifurcation of these islands which appears at resonant values. Resonances are defined as periodic and quasi-periodic orbits whose frequencies are in rational ratio with the fundamental frequency of the orbit of Europa around Jupiter, which is set to 1 in the normalized setting of the CRTBP.

Periodic orbits

Periodic orbits appear as forming the backbone of the dynamics, and offer a basic structure upon which to build the discussion of the parking solution regions.

The stability of a periodic orbit is conceived from the behavior of the periodic orbit variations. Therefore, the variational equations must be integrated for every periodic orbit of interest. The first order variations conform a linear differential system with periodic coefficients. As we know from Floquet's theory, its general solution is made of a linear combination of exponentials $e^{\alpha t}$ (or *characteristic multipliers*) whose coefficients are not constant, but certain periodic solutions with the same period T of the periodic orbit. Therefore, in order to determine the stability behavior of a periodic orbit (in linear approximation) it is enough to study the multipliers at the end of one period $\lambda = e^{\alpha T}$ (or the eigenvalues λ of the *monodromy* matrix).

The CRTBP is a Hamiltonian problem, and, therefore, the eigenvalues appear in reciprocal pairs $(\lambda, 1/\lambda)$. Further, periodic orbits enjoy one trivial eigenvalue $\lambda_0 = 1$ that, for Hamiltonian systems, has multiplicity 2. Then, periodic orbits of Hamiltonian systems with three degrees of freedom have 4 non-trivial eigenvalues, and two stability indices are normally used [14]

$$b_i = \lambda_i + 1/\lambda_i \qquad i = 1, 2 \tag{1}$$

The condition b_i real and $|b_i| < 2$ $(i = 1, 2)$ applies for linear stability.

When dealing with planar motions, one index measures the "horizontal" or in-plane stability (that we note $b_{\rm h}$), whereas the other (noted $b_{\rm v}$) shows the "vertical" stability character of the periodic orbit [15], that is the orbit's behavior when undergoing perturbations in the out-of-plane direction. There are critical values of the stability indices (some non-trivial eigenvalues taking the value $\lambda = \pm 1$) where new families of periodic orbits can bifurcate from the original one, either in the plane (critical horizontal index: $b_{\rm h} = \pm 2$) or orthogonal to it (critical vertical index: $b_{\rm v} = \pm 2$).

Note that at $b = +2 \Rightarrow \lambda = +1$, and the bifurcation occurs with the same period of the critical orbit. The case $b = -2$ implies that $\lambda = -1$ and $\lambda^2 = e^{\alpha(2T)} = 1$ resulting in a period doubling bifurcation. Besides the critical cases $b = \pm 2$, for $-2 < b < 2$ other families of periodic orbits may bifurcate with multiple period from the original one [16] (see also [17], [18]). Thus, for eigenvalues λ that are $n^{\rm th}$ roots of the unity

$$\lambda = \cos(2\pi\, d/n) + j \sin(2\pi\, d/n) \quad \Rightarrow \quad b = 2\cos(2\pi\, d/n), \tag{2}$$

where d and n are integer numbers and j is the imaginary unit, the corresponding stability index of the n-fold periodic orbit[‡] is $b = +2$. We call "d:n-resonant orbits" to these critical orbits, and "d:n-resonant families" to the families of periodic orbits that emerge from a d:n-resonant orbit.

The representation of the stability indices versus the parameter or integral generator of a family of periodic orbits produce what Hénon calls "stability curves" [16], where the changes in the stability of a family can be clearly appreciated. The stability curves are usually represented in the real plane. However, unstable orbits with complex eigenvalues out of the unit circle have complex stability indices. Therefore, in some cases we use three-dimensional stability curves. For a detailed description of the different cases of instability that can appear, the interested reader is referred to advanced textbooks on the topic or to the original reference [14].

Stability maps

While the bifurcation analysis of periodic orbits helps in establishing the relation between different stability islands, many families of periodic orbits belong to the same stability region, and grouping them together into one connected region helps to capture the notion of a stability region.

In order to combine alike families of periodic orbits and estimate the overall shape of the stability regions, the computation of stability maps has been considered [9]. These maps, based on the computation of a chaoticity indicator[§] known as the Fast Lyapunov Indicator (or FLI), allow us to to extend the information obtained via Poincaré maps in the 2-dimensional problem to the case of the 3-dimensional model. For each vertex of a grid of initial conditions (IC), the corresponding value of the FLI is computed, and a density map of the resulting array of values can be generated. For example, Figure 2(a) represents the stability maps computed for the same slice of IC as the one considered in the Poincaré map of Figure 1(a), while Figure 2(b) represents the stability map of the set of trajectories crossing the (x, z) plane orthogonally, thus showing a snapshot at the dynamics in the spatial problem.

In particular, we note that the larger the stability region, the larger is the robustness property of the central periodic orbit. For example, performing an impulsive maneuver along the x-axis from the nominal periodic orbit results in moving the IC of the nominal orbit along the V_x-axis. In the case presented on Figure 2(a), a ΔV of about $\sim$ 11 m/s is required to transfer a spaceraft from a nominal, stable, direct periodic orbit, to a higly chaotic region which will result in a high probability of impact[¶] with Europa after a few weeks without any control. Any ΔV smaller than this value

[‡] The T-periodic orbit after a period $\tau = nT$

[§] A chaoticity indicator is a map from the phase space to the set of real numbers, that allows us to distinguish between regular and chaotic trajectories, based on the indicator value.

[¶] or escape from Europa.

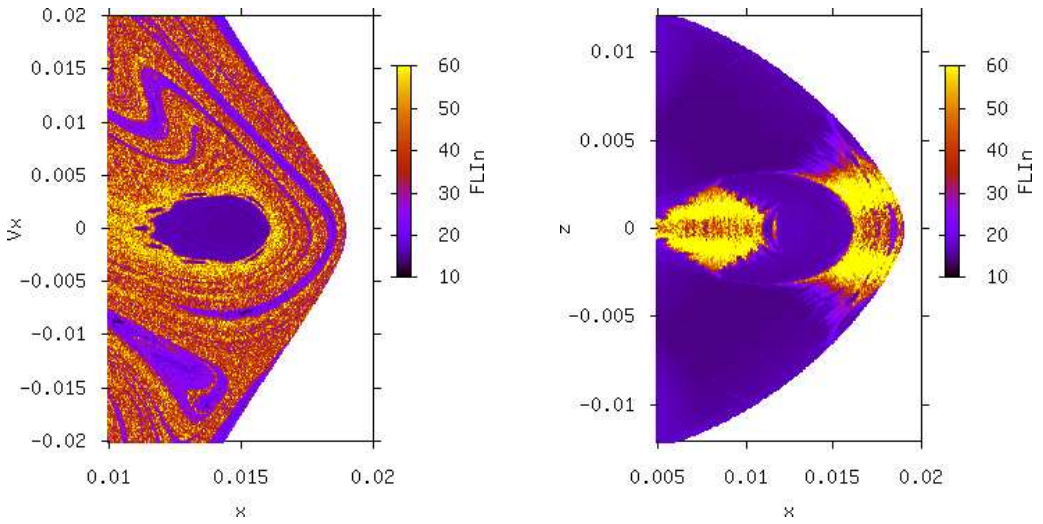

Figure 2: Examples of a FLI maps at fixed Jacobi constant ($C = 3.00363$) in the normalized Jupiter-Europa planar CRTBP ($\mu = 2.528^{-5}$). Low values of FLI indicate region of stability while large values indicate strong chaos. The chaotic sea is centered around the equatorial plane.

place the spacecraft on an orbit inside the stability region which will have the same characteristics as the nominal periodic orbit and will not create any impact/escape hazard.

Parking solutions evaluation

From the previous discussion, it appears that parking solutions can be characterized by a fundamental periodic orbit together with a notion of a robustness measure related to the volume of the stability region on a suitable section. The fundamental periodic orbit captures the main geometrical information of the stability region (shape of position path), and the robustness measure should capture the extent and shape of the overall stability region. While the use of a single number to summarize the robustness properties appears difficult to define, the description of the families of periodic orbits at the outer boundary of the stability regions, the computation of stability maps, as well as, the evaluation of the lifetime of sample trajectories in an ephemeris model does help in characterizing these complex dynamics.

Passing from the CRTBP to the ephemeris model requires some care. On one side, the ephemeris model is related to an epoch. However, since we are interested in long-term stability orbits, the epoch should be irrelevant to some extent, and we choose January 1, 2025 (Julian date of 2460677.0) for all our trials.

On the other hand, the orbit of Europa is not circular, but slightly elliptic. In fact, the distance from Europa to Jupiter varies due to eccentricity and slight perturbations in semi-major axis on the order of 1-2%. So we decided to do the transformation using the instantaneous angular momentum vector of Europa with respect to Jupiter, but introducing a one dimensional scaling parameter k that varies in the range 0.98 to 1.02. After scaling the initial state (position, velocity, and period) we do the propagation for a maximum of 1000 days, and plot the resulting "lifetimes," i.e. how long does it take to escape Europa or impact. Then, the stability of the orbit can be deduced for the width of the range of k values for which the orbiter reaches the required lifetime. The nominal value for the Europa-Jupiter distance is chosen to be 6.709×10^5 km, cfr. p. 347 of [19]. More details are given in Appendix.

PERIODIC ORBIT FAMILIES

There exist a great variety of families of periodic orbits of the CRTBP. However, since we are mainly interested in orbits enjoying long-term stability, we pay special attention to the family of equatorial retrograde orbits around Europa (hereafter, "the retrograde family") without limitting to the DROs case of [7, 8]. Of high interest is also the "direct family" of equatorial direct orbits around Europa, providing large regions of orbit stability for almost circular and egg-shaped orbits close to Europa. Among the less promising families investigated, only the halo family is described.

In general, we proceed as follows. After computing the main families of planar periodic orbits we, first, search for a variety of vertical bifurcations that occur at d:n-resonant orbits of a given family. Then, we continue each vertically bifurcated d:n-resonant family of three dimensional periodic orbits, and trace its stability behavior. A dense set of "critical" orbits where the stability of the corresponding d:n-resonant families change, helps in defining global stability regions in phase space [20].

Families of planar orbits

The retrograde family

The retrograde family starts with grazing, retrograde, equatorial orbits around Europa. For decreasing values of the Jacobi constant, the family continues with almost circular orbits of increasing size. Close to Hill's stability radius the orbits are no longer perturbed Keplerian ellipses around Europa, and, consequently, its shape also changes in the rotating frame, where we find ellipses with the semimajor axis in the y-axis direction and centered at Europa (see Fig. 3).

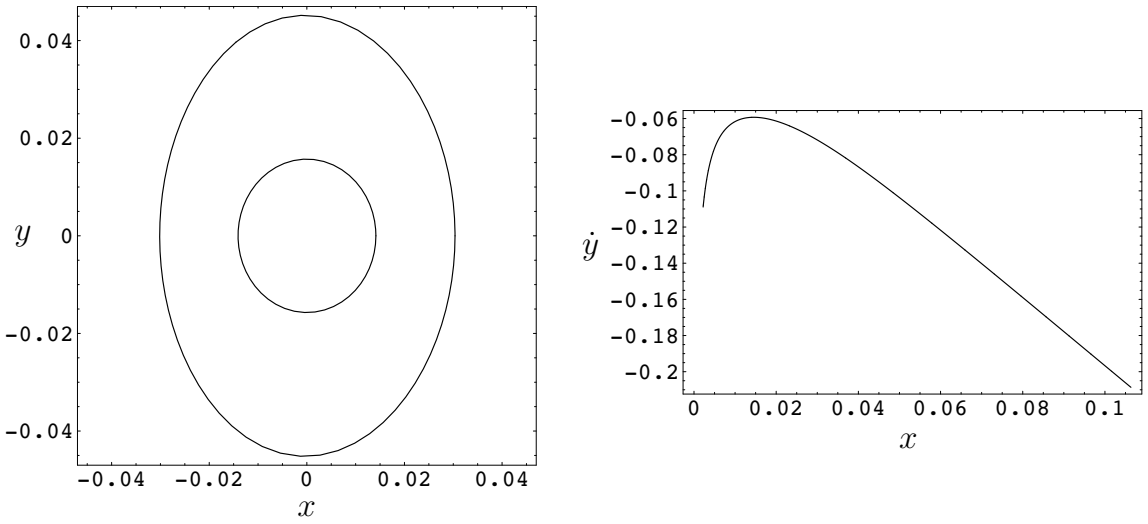

Figure 3: Retrograde family of periodic orbits around Europa. Left: sample orbits. Right: characteristic curve.

The orbits of the retrograde family are simple-periodic orbits that intersect the x-axis perpendicularly. Therefore, initial conditions of any orbit of the retrograde family can be chosen such that $x = x_0$, $y = z = 0$, $\dot{x} = \dot{z} = 0$, and $\dot{y} = \dot{y}_0$. Thus, the totality of the retrograde family can be represented by a "characteristic curve" $\dot{y}_0 = \dot{y}_0(x_0)$ [16]. That is the convention used in the right plot of Fig. 3, where we note that the minimum velocity $v = 0.0593017$ occurs at a distance $r = 0.0145519$ units of length (≈ 6.25 times the equatorial radius of Europa).

The left plot of Fig. 4 shows the stability curves (C, b) of Europa's retrograde family. In the

right plot we show an analogous curve where abscissas are x_0 distances. All the orbits are linearly stable, and, since neither b_h nor b_v take the critical values ± 2, we do not find any simple period or period doubling bifurcation of this family. However, as we will see later, we can find vertical and horizontal bifurcations for different multiplicities of the period.

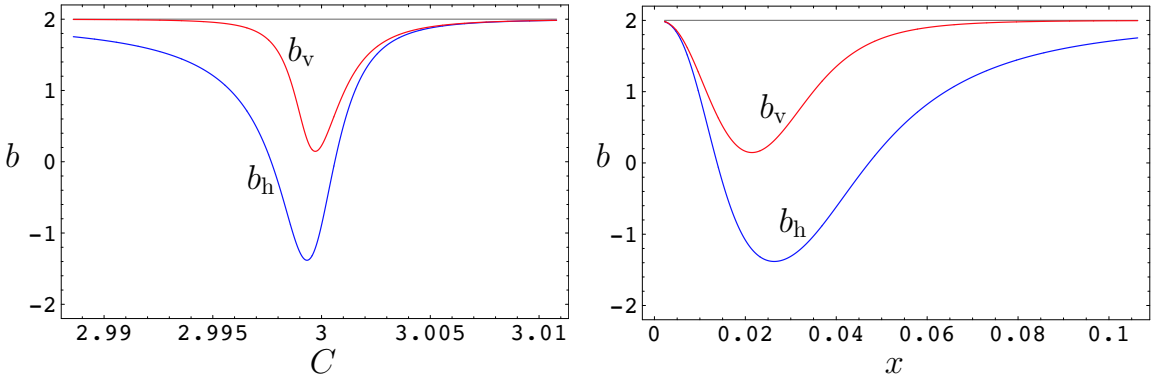

Figure 4: Horizontal (blue) and vertical (red) stability indices of the retrograde family. Left: variations of the Jacobi constant. Right: distance (x_0) variations

The direct family

Starting from a planar, equatorial, direct periodic orbit close to Europa, we can continue the "direct family". Figure 5 shows a portrait of the direct family that includes only nonimpact trajectories. The stability curves of the direct family are shown in Fig. 6.

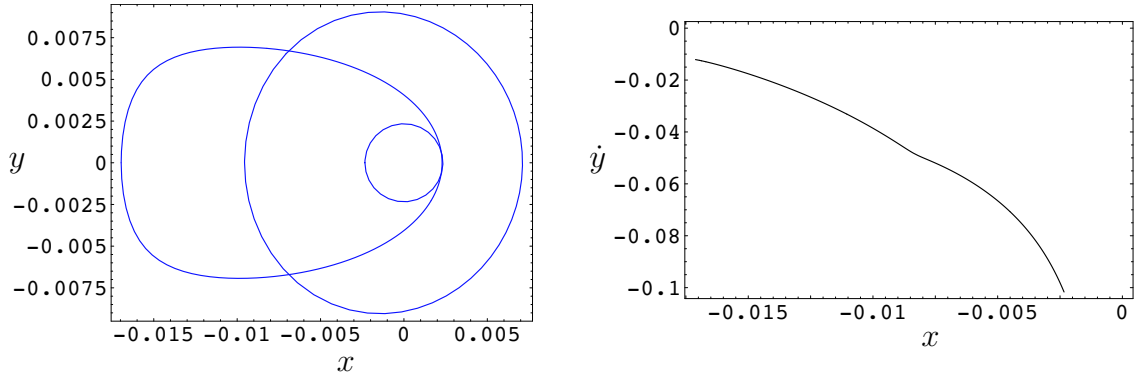

Figure 5: Direct family of periodic orbits around Europa. Left: sample orbits. Right: characteristic curve.

Close to Europa, the orbits are low ellipticity ellipses centered at Europa with the major axis in the ordinates direction. Decreasing values of the Jacobi constant produce ellipses of increasing size. Both stability indices decrease slowly until the horizontal one reaches a relative minimum $b_\mathrm{h} = 1.6515$ at $C = 3.00432$; the axes of the corresponding ellipse are $r_m = 0.00690716$, $r_M = 0.00722138$ ($r_m = 4631.51$, $r_M = 4842.21$ km). At this point, the shape of the orbits change from low ellipticity ellipses to egg-shaped orbits with the basis towards Jupiter (direction of negative abscissas). The egg-shaped orbits become more and more exagerated until impact with the surface of Europa at $C = 3.0036$ (vertical line in Fig. 6). The evolution of this family for decreasing values of the Jacobi constant is similar to Darwin's "Family A of Satellites" [22] and Broucke's analogous family H_1 [23] (or Henon's g' family of the Hill problem [15]), with highly unstable orbits, and passing through

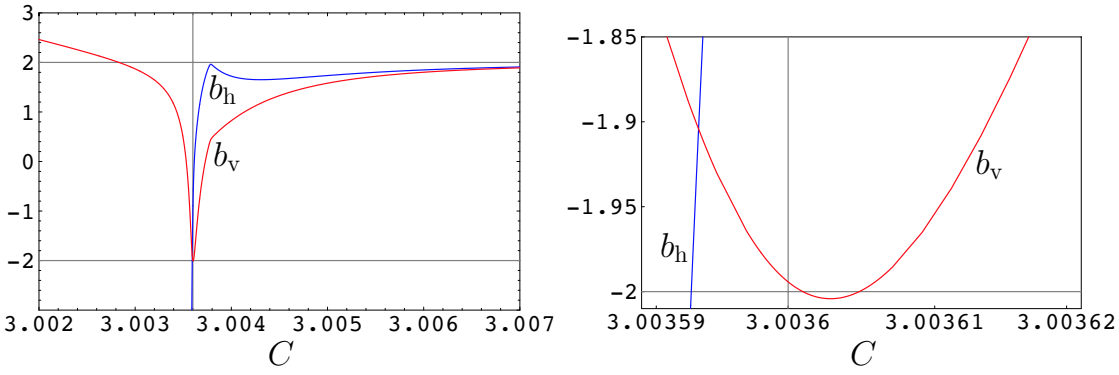

Figure 6: Left: Stability curves of the direct family. Right: Detail.

several collissions —that is not of interest for the subject of this paper. Note in the detail of Fig. 6 the two vertical, period doubling bifurcations ($b_v = -2$) that occur close before the egg-shaped orbits impact Europa.

Other families

Other families of planar orbits can be computed starting from small ellipses around the (unstable) collinear points [12]. The collinear points are placed in the x axis, at $x = 0.020485$ and $x = -0.020211$. We do not pay attention to the third collinear point. We call the L_2 family to the family of planar, periodic orbits that surround the collinear point L_2 (positive x). It exists for decreasing values of C. Figure 7 shows a portrait of the L_2 family that includes only nonimpact trajectories. The bottom-right plot of Fig. 7 shows the corresponding stability curves, where we note that all the orbits behave with high instability against in-plane perturbations ($|b_h| \gg 2$). In general, the orbits also present instability with respect to out-of-plane perturbations, but there is a small region where the vertical stability index is $|b_v| < 2$.

The orbits of the L_1 family are almost symmetric with respect to the y axis to those of the L_2 family, with a similar behavior.

Bifurcations of families of 3-D periodic orbits

We compute bifurcations of the previously computed families of planar, periodic orbits for different multiplicities of the period by using Eq. (2). However, first of all we must note that not every resonance is always possible. That is the case of the retrograde family. As previosly noted, we do not find simple period (1:1-resonance, $b = +2$) or period doubling (1:2-resonance, $b = -2$) bifurcations of the retrogade family. Furthermore, as appreciated in Fig. 4, the minimum value $b_{v,m} \approx 0.146$ of the vertical stability index limits the possible resonances to

$$\frac{d}{n} = \frac{1}{2\pi} \arccos\left(\frac{b_{v,m}}{2}\right) \approx \frac{41}{172} < \frac{1}{4}.$$

On the contrary, we can find bifurcations on the plane further away than the 1:4-resonance. However the minimum value $b_{h,m} \approx -1.38$ of the horizontal stability index, again limits the horizontal resonances that can occur to $d/n \approx 13/35$. Furthermore, due to these minima, we find two different bifurcations for each allowable d:n-resonance, except for exactly the value $b_{v,m}$ or $b_{h,m}$. For example, as appreciated in Fig. 4, $b_v = 1$ for both $C = 2.99871$ ($x_0 = 0.0349429$) and $C = 3.00107$ ($x_0 = 0.0114464$). Then, as derived from Eq. (2), we found two different 1/6-resonant orbits, which give rise to two different families of three dimensional periodic orbits that repeat themselves after $6-1 = 5$ crossings of the x-y plane in the upwards direction, or "cycles". This example is illustrated

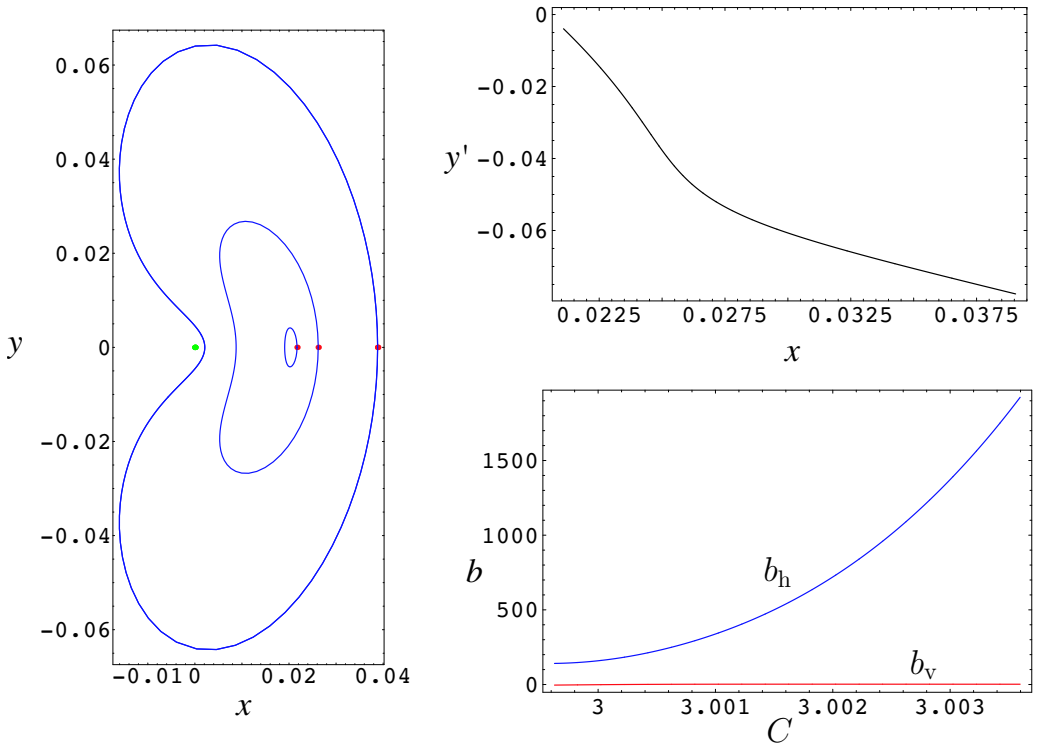

Figure 7: Left: Nonimpact orbits of the L_2-family. Right: characteristic (top) and stability (bottom) curves

in Fig. 8, where we note that close to Europa (left plot), the orbit is almost circular remaining approximately between 7500 and 8000 km from Europa, while far away from Europa the orbit remains between 23200 and 37500 km from Europa (right plot).

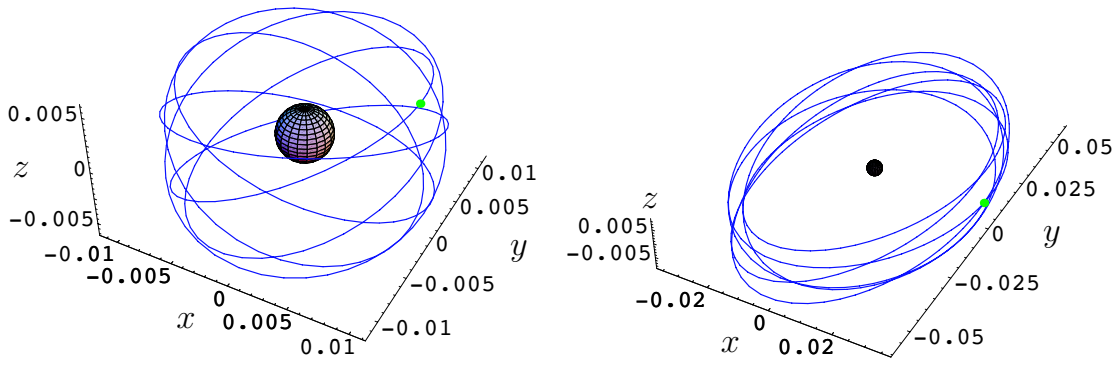

Figure 8: Periodic orbits after 5 nodal periods close to (left) and far away from (right) Europa. Note the different scales

Vertical biburcations of the retrograde family

To study the three dimensional motion in a dense region around Europa we compute many families of three dimensional periodic orbits bifurcated at different resonances. Some of them are detailed in the Appendix.

Following Hénon [15], we can find vertically bifurcated orbits with simple period at $x \neq 0$, $y = 0$,

either with $z \neq 0$, $\dot{z} = 0$ (Hénon's type $C_{\rm v}$), or with $z = 0$, $\dot{z} \neq 0$ (Hénon's type $B_{\rm v}$). All the critical orbits we computed are multiple periodic orbits, and we find both types of bifurcations.

Close to Europa, the families of three dimensional periodic orbits show a typical behavior. Starting from a near circular, equatorial, retrograde, periodic orbit that is resonant after n periods in the rotating frame and d rotations of Europa, a small perturbation either in the z (type $C_{\rm v}$ bifurcation) or in the $\dot{z}$ (type $B_{\rm v}$ bifurcation) direction produce a three dimensional orbit that is periodic after $n - d$ cycles. Then, increasing values of the Jacobi constant produce three dimensional orbits with decreasing inclination that evolve from retrograde to direct motion through the 180° of inclination.

Figure 9 presents the stability curves of several families close to Europa. As inclination angle, we use the inclination in degrees

$$i = \arctan(\dot{z}_0/\dot{y}_0) \tag{3}$$

of the velocity vector at the point $y_0 = z_0 = 0$, where $\dot{x}_0 = 0$. This angle provides a measure very similar to the averaged inclination for perturbed Keplerian ellipses, and is an illustrative quantity for describing the evolution of non Keplerian orbits. Note in Fig. 9 that, within the numerical precision, The index b_2 always take the degenerate value $b_2 = +2$. This index is related to intrinsic displacements in the (instantaneous) out of plane direction, with the result of some indefinition in the argument of the node in the rotating frame of the three dimensional orbits.

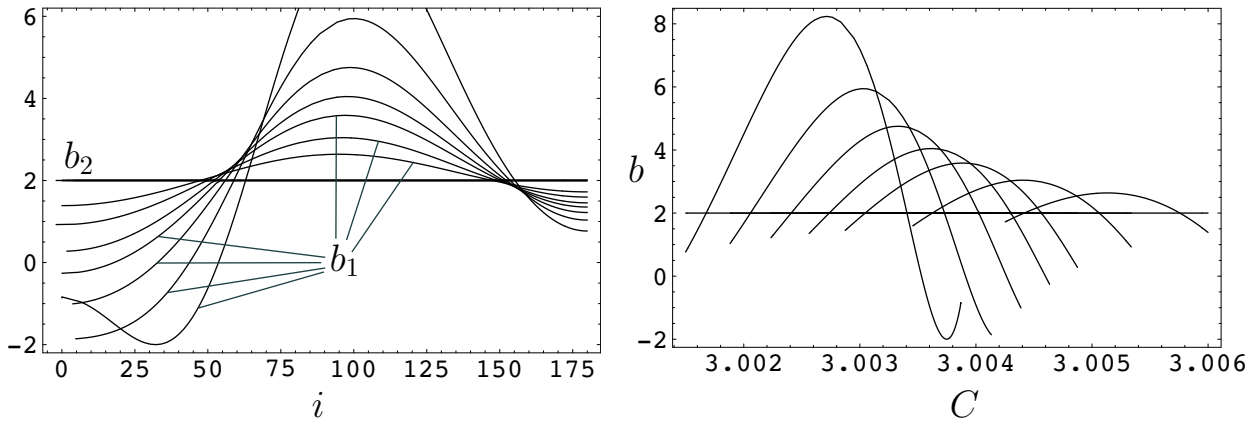

Figure 9: Right: Inclination-stability curves of the 1:7-, 1:8-, 1:9-, 1:10-, 1:11-, 1:13- and 1:16-resonant families of the retrograde family close to Europa. Left: Same curves plotetd as a function of the Jacobi constant.

Near circular orbits change their stability character at certain critical inclinations i_c, and, for the computed families, we find large areas of instability centered around polar orbits, yet slightly displaced to highly inclined retrograde orbits ($i \sim 100°$). The changes in the stability properties of almost circular orbits are related with bifurcations of stable eccentric orbits.

Far away from Europa, d:n-resonant families exist for decreasing values of the Jacobi constant. In the rotating frame, the three dimensional orbits remain approximately on the surface of an elliptic cylinder that increases its height for decreasing values of the Jacobi constant. The height of the cylinder is directly related to the velocity inclination Eq. (3), and at certain height/inclination the periodic orbits change to instability. The left plot of Fig. 10 presents the stability curves of several families far away from Europa in terms of the velocity inclination, where we note the abrupt change in orbit stability at certain critical inclination. The minimum retrograde inclination for which the orbits are stable decreases for increasing distances to Europa. However, starting from the 1:19-resonance, a region of mild instability appears which size increases with distance.

By joining a dense set of points (x_0, i_c) corresponding to the different d:n-resonant families, we

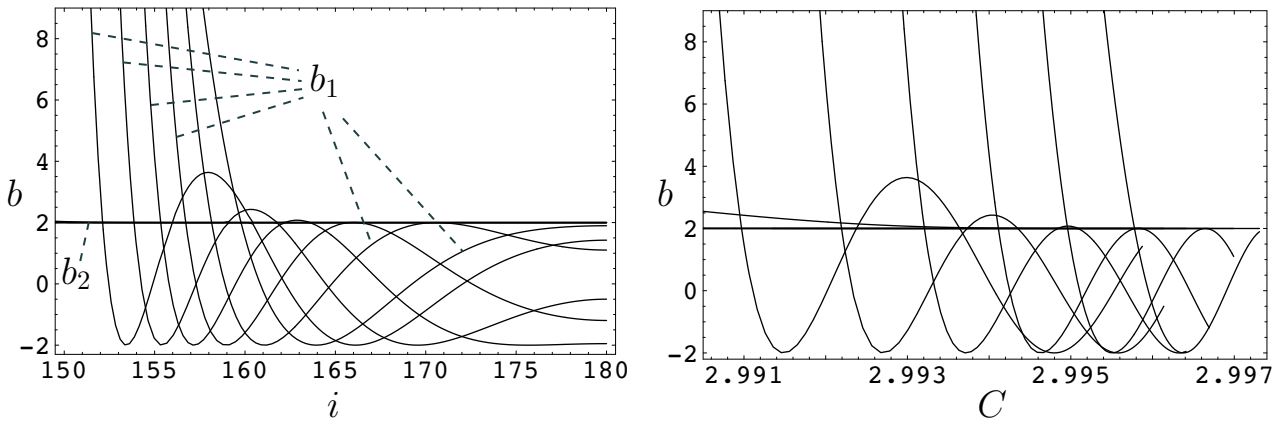

Figure 10: Left: Inclination-stability curves of the, from left to right, 1:23-, 1:21-, 1:19-, 1:17-, 1:15-, and 1:13-resonant families far away from Europa. Right: Same curves plotted as a function of the Jacobi constant.

can define stability regions in three-dimensional space as presented in Fig. 11, where the vertical axis marks the boundary ($d/n \approx 41/172$) between resonances close to, and far away from Europa. In the far away case the (x_0, i_c) points correspond to the change to strong instability.

Figure 11 is in good agreement with the "Red Sea Plot" of Lam and Whiffen (see Fig. 14 of [8]) that presents a neck in the stability region between 14000 and 24000 km approximately, corresponding to the irregular area of Fig. 11, and with an abrupt minimum around 22500 km corresponding to the peak at the 1:6 resonance in Fig. 11. Then, the narrow yellow region of [8] corresponding to orbital lifetimes of ≈ 25 days, can be fitted to the cubic

$$i_c = 138.097 + 2136.79\, x_0 - 45831.7\, x_0^2 + 246110.\, x_0^3$$

The agreement between Fig. 11 and Lam and Whiffen's "Read Sea Plot" deteriorates far away from Europa. Note, however, that both figures are not directly comparable, and we find much better agreement when considering long lifetimes orbits of the CRTBP [21] instead of restricting to stable periodic orbits.

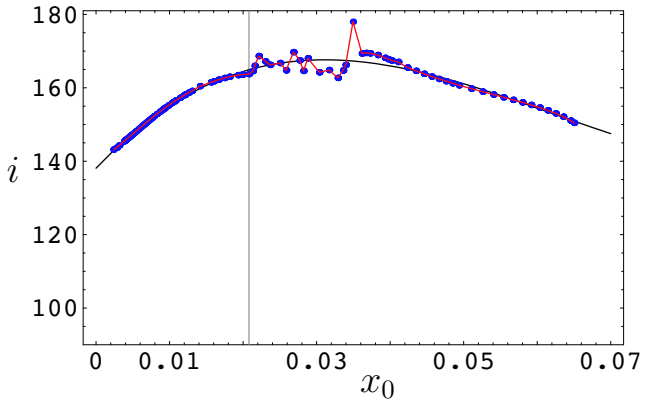

Figure 11: Boundary of the region of strong instability around Europa.

Vertical biburcations of the direct family

Analogously to the case of retrograde orbits, a variety of d:n-resonant families can be computed from the direct family. Note, however, that, as shown in Fig. 9, many of them have been already computed in the case of retrograde motion close to Europa. Then, as before, we compute a set (x_0, i_c) of points that define a stability region for direct, almost circular, three-dimensional motion close to Europa as before. Figure 12 presents the complete picture for the stability properties for these type of orbits.

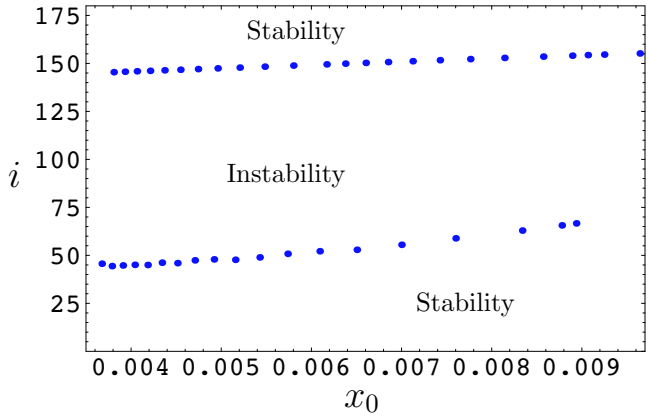

Figure 12: Stability regions for almost circular motion close to Europa.

Note in Fig. 12 (see also in Fig. 9) the difference between the stability regions in the direct and retrograde case: While the angle α between the orbit at the "critical" inclination i_c and the equatorial plane decreases with the distance to Europa for retrograde orbits ($\alpha = 180^\circ - i_c$), it increases with distance for direct orbits ($\alpha = i_c$).

For almost circular, direct motion we should limit to resonant families below the 1:6-resonance, where the orbits are clearly egg-shaped and the inclination information as defined in Eq. 3 must be used with care. The limit for d:n-resonant families of non impact, direct, egg-shaped, three-dimensional periodic orbits is a period doubling bifurcation ($b_v = -2$) that occurs at $C = 3.003605$ (see the detail of Fig. 6). The stability curves of the corresponding family of periodic orbits is presented in Fig. 13. For decreasing values of the Jacobi constant, the three dimensional, egg-shaped, periodic orbits are stable until they change to instability at $C = 3.00348$ into a Krein collision of the eigenvalues —where the four nontrivial eigenvalues abandon the unit circle out of the real axis— and the stability indices take complex conjugated values. At $C = 3.00207$ the stability indices change to real. The family continues with unstable orbits until it suffers from a reflection at $C = 3.00205$. The rest of the family exists for increasing values of C, and is made of unstable three dimensional orbits that terminates at $C = 3.00253$ on a (highly unstable) planar orbit of a new family. The orbits of this new family are planar, direct, egg-shaped, periodic orbits with the basis towards the positive x direction that are almost symmetric to the orbits of the previously computed egg-shape family, and with an analogous behavior. We note, however, that the simply periodic egg-shape orbits with this orientation are also stable. We delay details to a future paper, and only computed several three dimensional periodic orbits bifurcated from the egg-shape families at different d:n-resonant orbits. Figure 14 shows an example.

As appreciated in the detail of Fig. 6, there is another vertical, period doubling bifurcation of the direct family at $C = 3.003601$. The stability curves of the corresponding bifurcated family are presented in the left plot of Fig. 15. This new family exists for decreasing values of the Jacobi constant with orbits of increasing size and inclination that, in general, are unstable. However, there

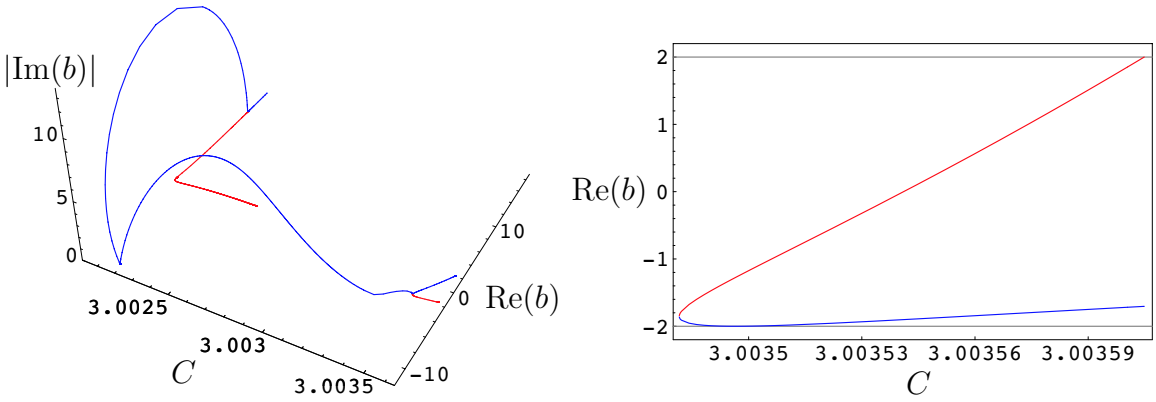

Figure 13: Left: Stability curves of the 1:2-resonant family of egg-shaped periodic orbits. Right: detail in the region of stability

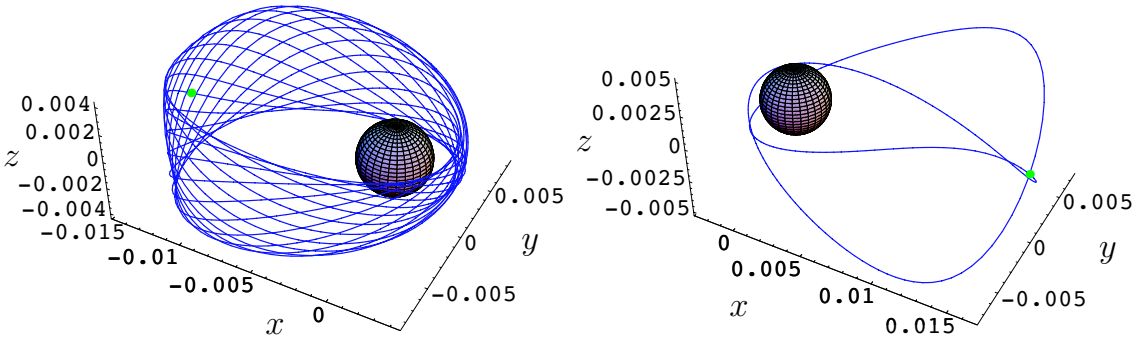

Figure 14: Stable egg-shaped orbits. Left: 6/17-resonant. Right: 1/2-resonant

is a narrow region of stability for $2.99943 < C < 2.99992$. The stable orbits show retrograde motion remaining at a distance between 8 and 15 radius of Europe aproximately, and with an inclination parameter $i \approx 165°$.

Other families

Despite the L_1 and L_2 families are highly unstable, we find two vertical bifurcations and continue the corresponding families of three-dimensional periodic orbits.

Thus, in reference to the L_1 family, we find a vertical, bifurcation at $C = 3.00094$ ($b_v = -2$), that produces eight-shaped orbits with increasing unstability. The other vertical bifurcation occurs at $C = 3.00333$ ($b_v = +2$), and gives rise to the 'Halo' family. The continuation of the Halo family to decreasing values of the Jacobi constant reaches a minimum at $C = 3.00084$ (see the left plot of Fig. 16) with a reflection in a small region of stable orbits. The orbits of the family continue with increasing values of C until they impact the surface of Europa at $C = 3.00108$. The right plot of Fig. 16 shows a stable orbit for $C = 3.00084$; due to symmetries in the model, we also find a symmetric solution with respect to the x-y plane.

The behavior close to the L_2 point is almost symmetric to the L_1 case, and we do not give details here.

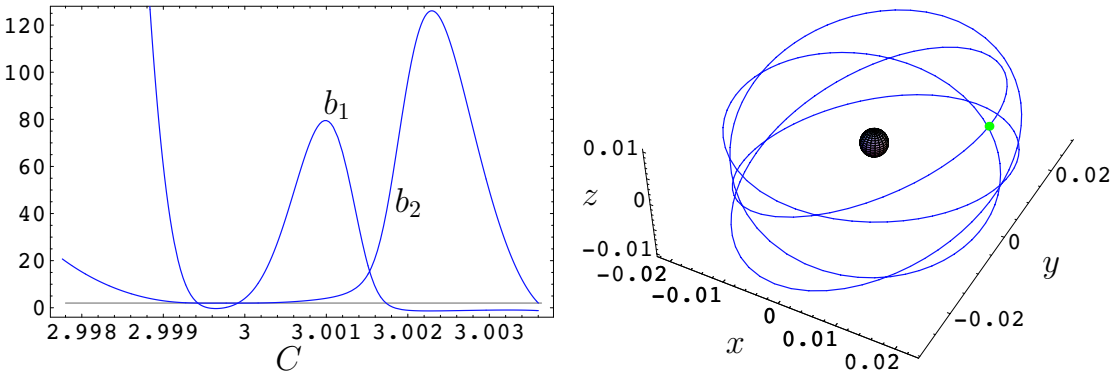

Figure 15: Left: Stability curves of the family bifurcated at $C = 3.003601$ from the direct family. Right: Sample orbit inside the region of stability.

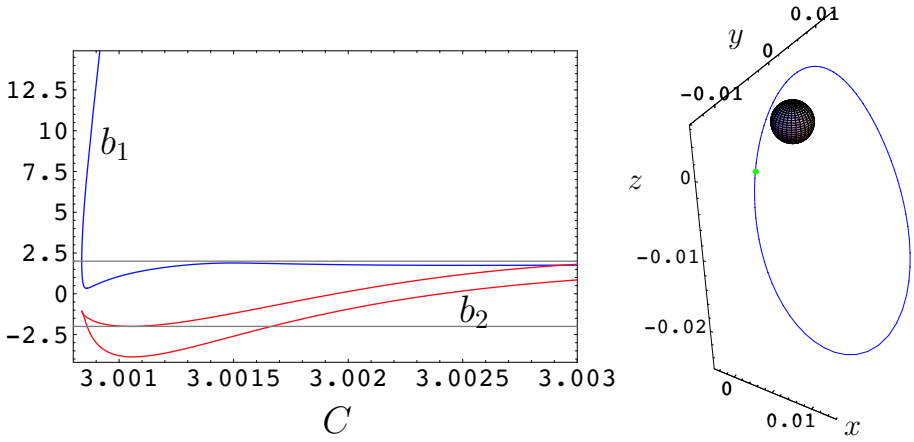

Figure 16: Left: stability curves of the Halo L_1 family. Right: sample stable orbit

STABILITY REGIONS

From the previous discussion, it appears that four main, large, stability regions centered around the DRO, direct egg-shaped and halo families exist. At a fixed Jacobi constant, the stability region are 5-dimensional volumes in phases space, which can be characterized by a 4-dimensional volume of initial conditions. Instead of considering all of the six, 2-dimensional projections of the different maps on the coordinates planes, a good idea of the size and main characteristics of these regions can be obtained by simply considering a few maps around some selected periodic orbits. For each periodic orbit considered, two stability maps are generated; one map describing the section of the stability region when the position is varied with a fixed velocity direction, while the other map considers the variations in velocity angle at a fixed position. The half-width of the stability regions shown on this last type of variations indicates the approximate amount of ΔV needed to transfer a spacecraft out of the center of the stability islands and, thus, the robustness properties of the most stable trajectories in the region considered[‖]

[‖]Note that, the actual ΔV corresponding to a half-width of a stability island indicated by these maps is different from the value read on one axis of the axis, as the maps considered are generated at a fixed position and Jacobi constant, so that the overall velocity magnitude must remains unchanged. A ΔV along the $\dot{x}$ coordinate has to be corrected by a ΔV in another direction, $\dot{y}$ or $\dot{z}$, in order to keep the velocity magnitude unchanged. Denoting $\Delta\bar{V}$ the reading of the half width on one of these maps on one of the coordinate axis used (e.g $\dot{x}$), and V the velocity magnitude at the state considered, the ΔV needed to exit the stability region at the same Jacobi constant is given by $\Delta V^2 = 2V^2 - 2\Delta V^2\sqrt{1-\left(\Delta\bar{V}/V\right)^2}$. This last expressions is approximately $\Delta\bar{V}$ when the ratio $\Delta\bar{V}/V$ is small.

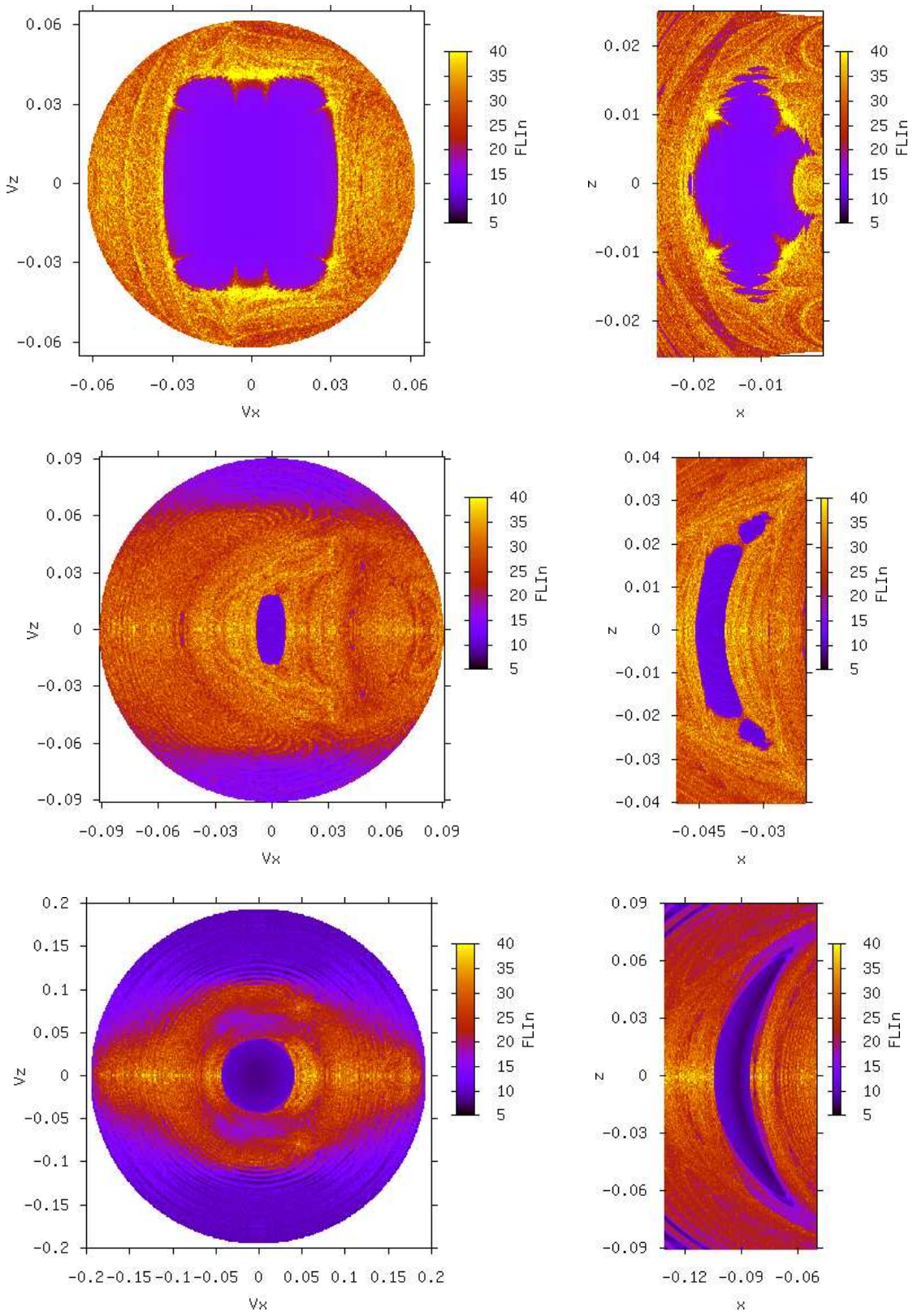

Figure 17: Sample FLI maps around DRO. Left column: Velocity variation, fixed position. Right column: Position variation, fixed velocity. From top to bottom (by row): C = 3.0014, region close to Europa; C = 2.9982, neck region; C = 2.9911, far away region.

Retrograde regions

In the retrograde case, we have seen that the planar DRO family is stable and the associated bifurcated families of 3-dimensional periodic orbits are also stable up to a certain inclination, the stability region encompassing these orbits thus appears as centered around the equatorial plane, and highly inclined trajetorie s appears as lying in a large chaotic sea.

Figure 11 indeed captures this idea and shows some of the complications that appear in a "neck", or transition, region extending from $x_0 \simeq 0.02$ and $x_0 \simeq 0.044$. The examination of the stability-inclination curve of the 1:23 and the 1:21 resonance hints at the existence of independant stability regions, as these families present several transitions from a stable to unstable character.

Figures 17 and 18 present a few sample maps aroud the (x, z)-plane crossing, $x < 0$ of the DRO family. For each case, the position variations are obatined by changing the x and z coordinates** at a fixed Jacobi constant, while the velocity variations are captured by varying the $\dot{x}$ and $\dot{z}$ coordinates†† (Jacobi constant fixed). From these maps‡‡, it appears that the DRO family lies indeed at the center of a large stability region symmetric about the equatorial plane and limited in the maximum out-of-plane motion by unstable motion (Figure 17, top and bottom plots). In the neck region (Figure 17 middle plot and Figure 18), the main stability region is much smaller in all its dimensions and is surrounded by even smaller, disconnected, stability islands. The trajectories near the center of the main stability island are very stable but require the use of large ΔV maneuvers to be accessed. Thus, the smaller stability islands in the neck region may represents more suitable parking solutions as, some of them, present good stability properties and may be easier to transfer to.

While the central, equatorial, stability region mostly dominates the picture in the retrograde case, in the neck region, the width of this region shrinks to zero in the equatorial direction at two different Jacobi constants for which the planar, unstable 1:3 resonant periodic orbits bifurcate from the main DRO family. The stability region associated with the DRO family remains connected over the entire C range, but the connection only exists through purely 3-dimensional motion near the critical neck values. This disapearance of the central region allows the shape of this central stability region to change from the close to the far away region. We note, however, that the largest width of the stability region always appears in the z and $\dot{z}$ directions, equatorial orbits being thus less robust with respect to in-plane perturbations than out-of-plane accelerations.

Direct and halo regions

In the direct case, the stability region associated with direct, almost circular orbits close to Europa is rather large, centered around the equatorial plane and resemble the stability region on the retrograde side at equivalent Jacobi energies. This is clearly captured by Figure 12.

As C decreases, however, the evolution of this main stability region proceed differently than in the retrograde case. While the chaotic sea of the highly inclined trajectories grows and reduces the size of the retrograde, main stability region to more and more equatorial orbits, the stability region in the direct case starts to disappear from the equatorial plane. This is in part due to the influence of the transit dynamics associated with the libration points region. Indeed, the stable and unstable manifolds tubes originating from these regions correspond to direct motion when the zero velocity surface starts to open up [25]. The extent of the destruction of the stability regions can be clearly appreciated on Figure 19 which represents a set of stability maps around the (x, z)-plane crossing, $x > 0$, of the a few periodic orbits in the direct family.

We note that the transition from the large connected stability region, that exists close to Europa at large values of C, to a completely chaotic dynamics occurs in a very small range of Jacobi constant (see Figure 19. Starting from the equatorial plane, the transition follows a complex scheme.

** One can think of these maps as a C_v type families of periodic orbits.

†† These maps can be thought os as capturing the B_v type families of periodic orbits.

‡‡ and the computation of many more not printed here for paper size limitations constraints

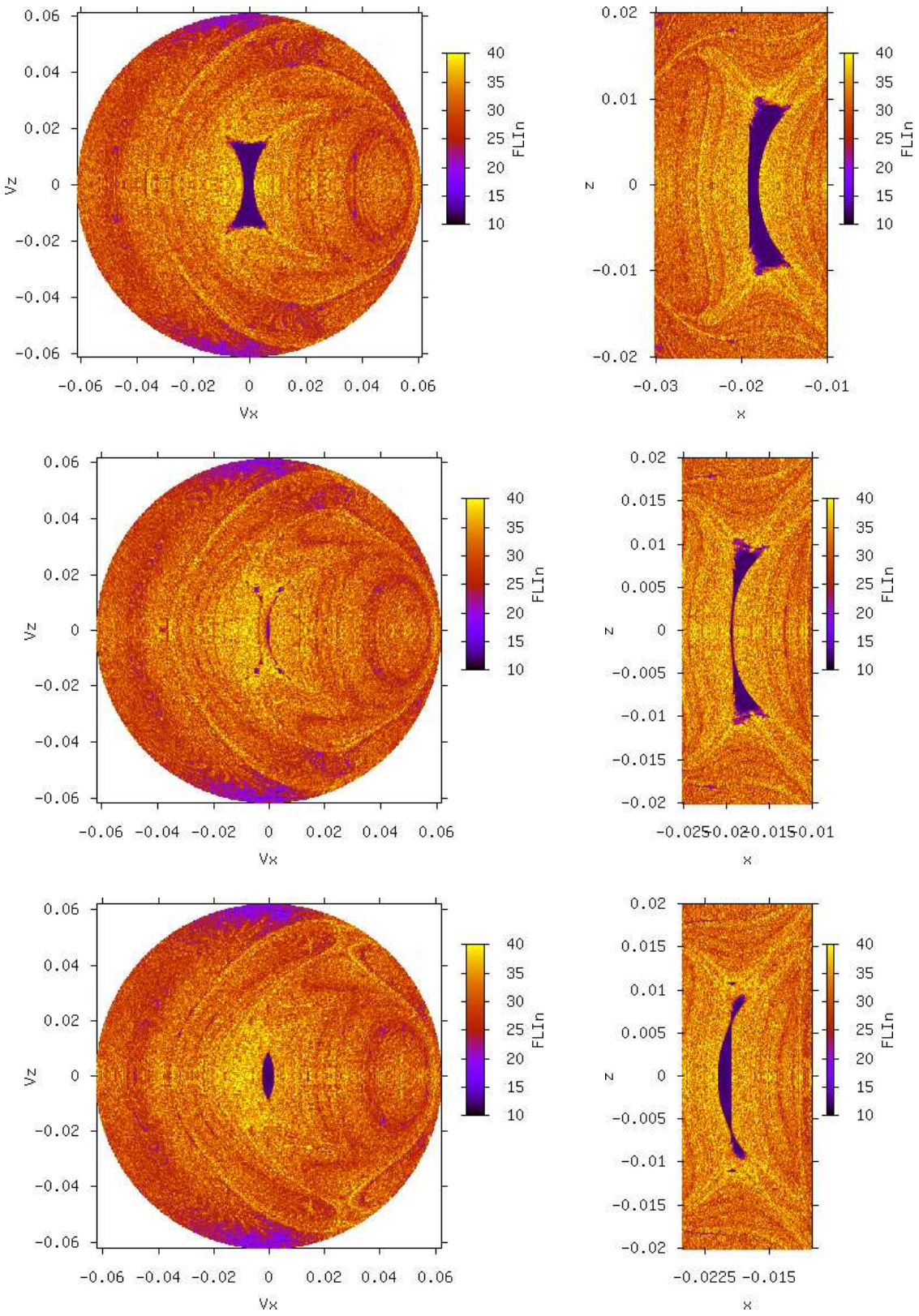

Figure 18: Evolution of the stability region at one of the critical neck values. Left column: Velocity variation, fixed position. Right column: Position variation, fixed velocity. From top to bottom (by row): C = 3.0000, C = 2.9999, C = 2.9998

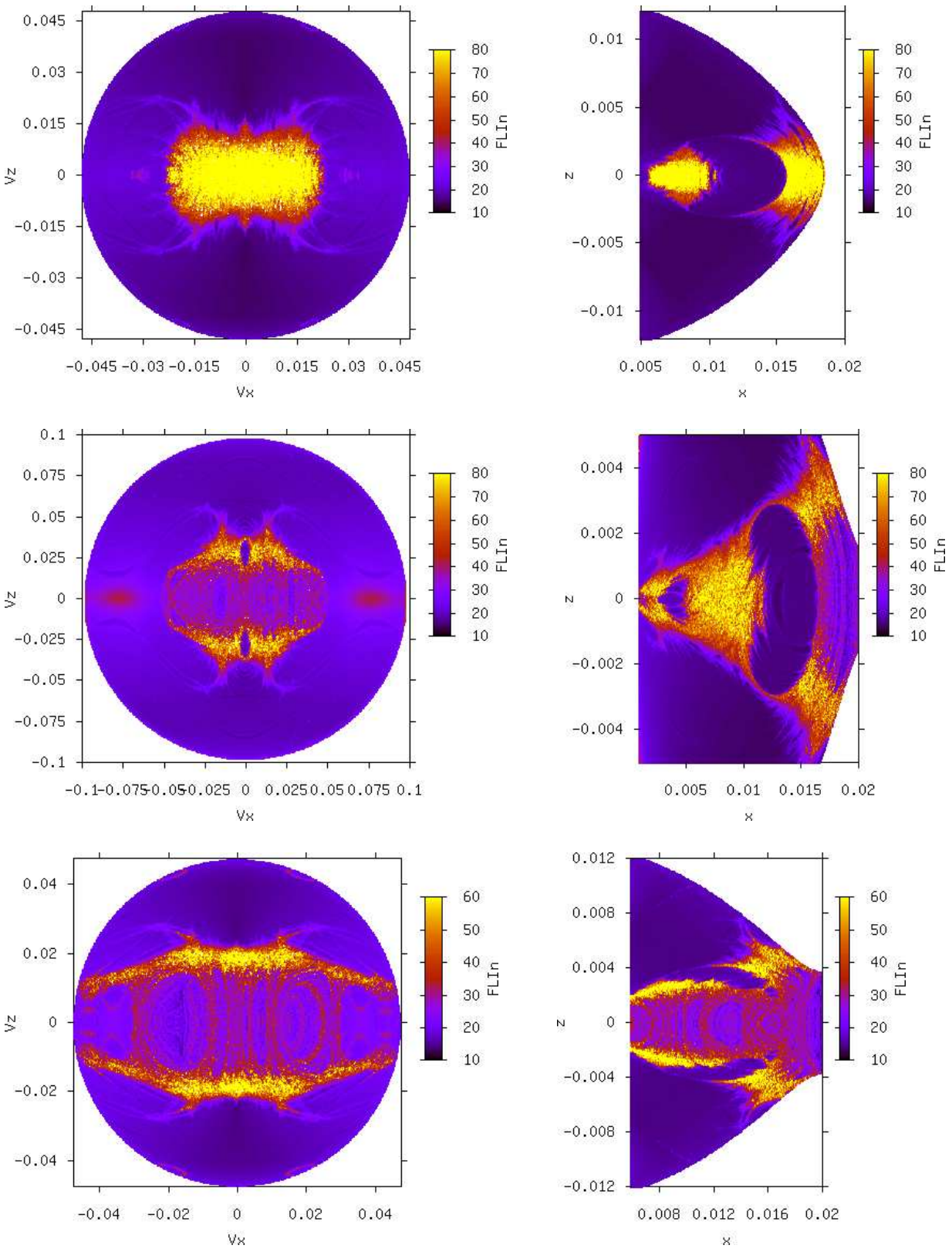

Figure 19: Sample FLI maps for the direct families. Left column: Velocity variation, fixed position. Right column: Position variation, fixed velocity. From top to bottom (by row): C = 3.00364; C = 3.0036 ; C=3.00355.

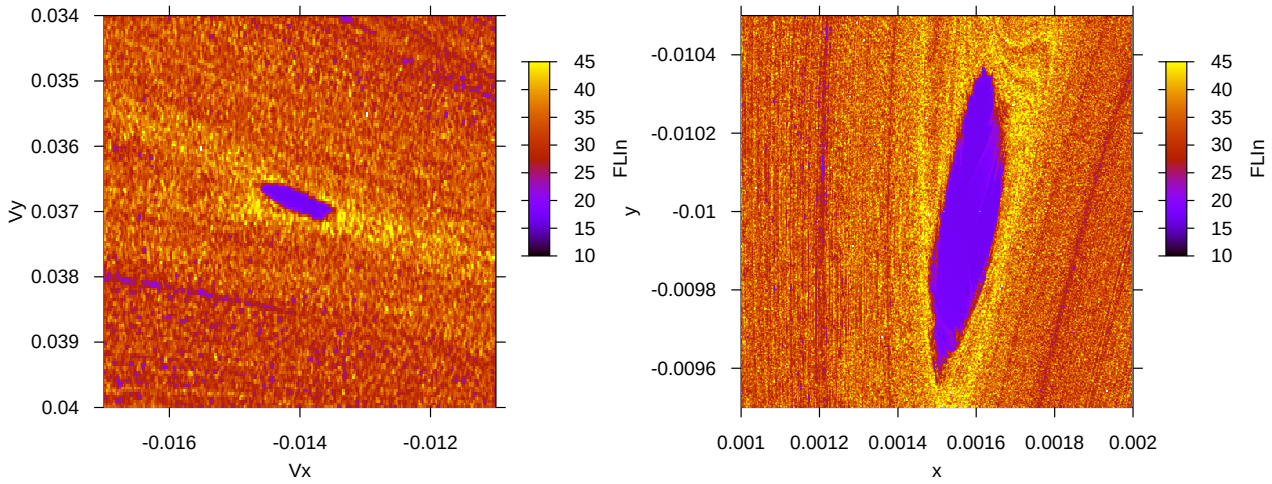

Figure 20: Sample FLI maps for the halo family around a halo orbit at $C \simeq 3.00084$. Left column: Velocity variation, fixed position. Right column: Position variation, fixed velocity.

Finally, the case of the change in stability in the halo families near Europa results in a small stability island at rather small Jacobi constant values. The size of the stability patched are on the order of a couple of hundreds of kilometer, the largest width being in the y-direction, as shown on Figure 20.

These small stability islands are the latest remanents of the destruction of the main direct region by the unstable dynamics originating from the libration points, showing the complex connections between the different dynamical regimes present in the restricted problem.

EPHEMERIDES RUN

A sample of initial conditions are mapped from the CRTBP to a true ephemeris state at a arbitrary epoch as explained in the Background section. The ephemeris files, active bodies, and associated masses are provided in Appendix. The intent is not to independently analyze the full phase space using an ephemeris model. Rather, it is to validate the notion that the size of a stability island in the CRTBP is indeed correlated to the robustness of a solution in the ephemeris model. The stability islands of interest come from the generation and stability analysis of neighboring resonant families that bifurcate from the main simple period planar families. Figure 21 gives the evolution of the distant retrograde family of the 1:23 resonance. As expected, the volume of the stability region appears to shrink with inclination as indicated by the average lifetime for the 50 different mappings. The orbit (a) on that figure is stable for the full 1000 days for the full range of the k scaling factors. As the inclination increases and the family movezs towards the boundary of the stability region (cases (b) and (c)), the size of the long-term stability regions decreases. Note that a region of at least 1000 day solutions is evident in case (d) hinting at the existence of a disconnected stability island at this energy. This is consistent with the FLI map in Fig. 17, bottom plot, and with the left curve in Fig. 10.

Figure 22 gives two examples of retrograde stable solutions, the first case, Fig. 22(a) is part of

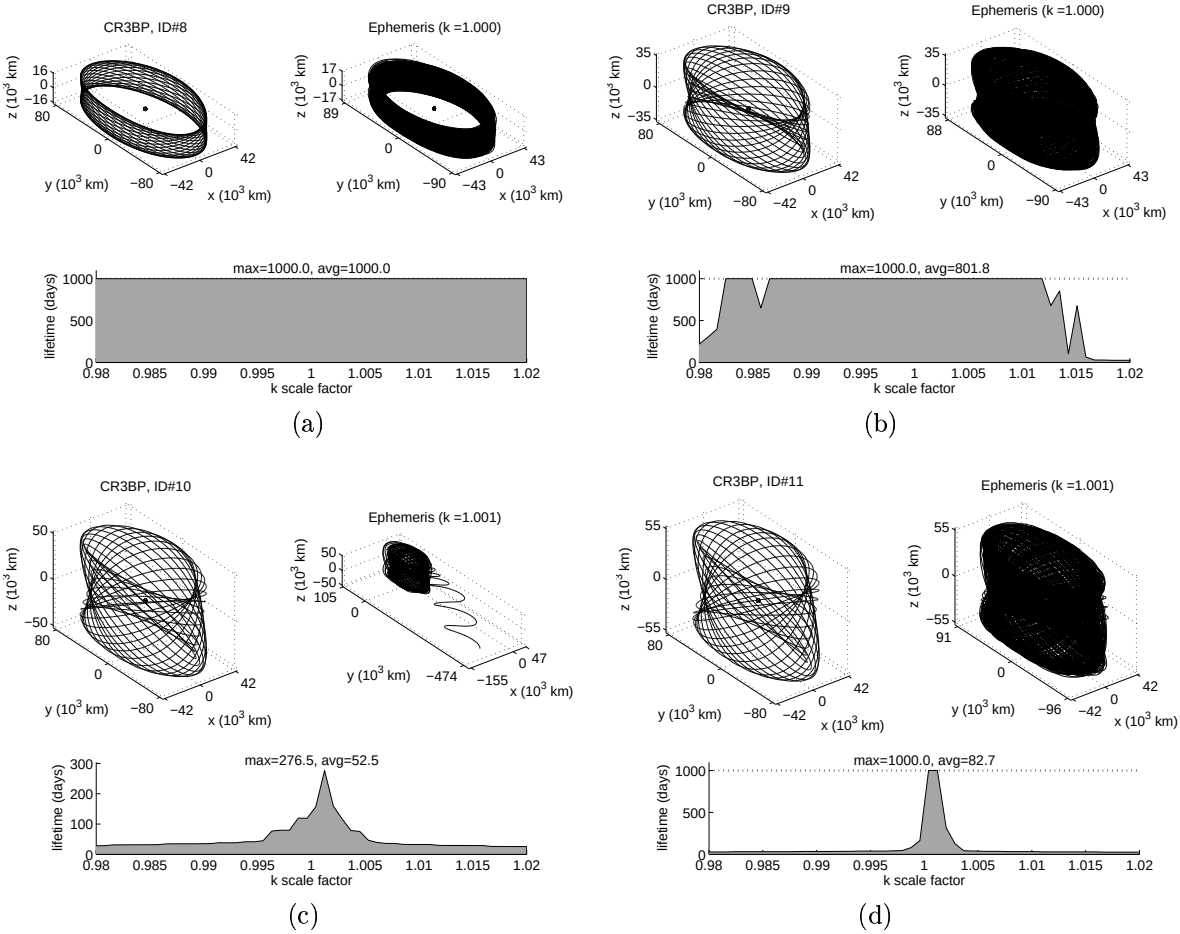

Figure 21: Evolution of the 1:23 family of ephemeris model retrograde periodic orbits. The average lifetime indicated is a scalar metric of the robustness of a stability island/region. See Background section.

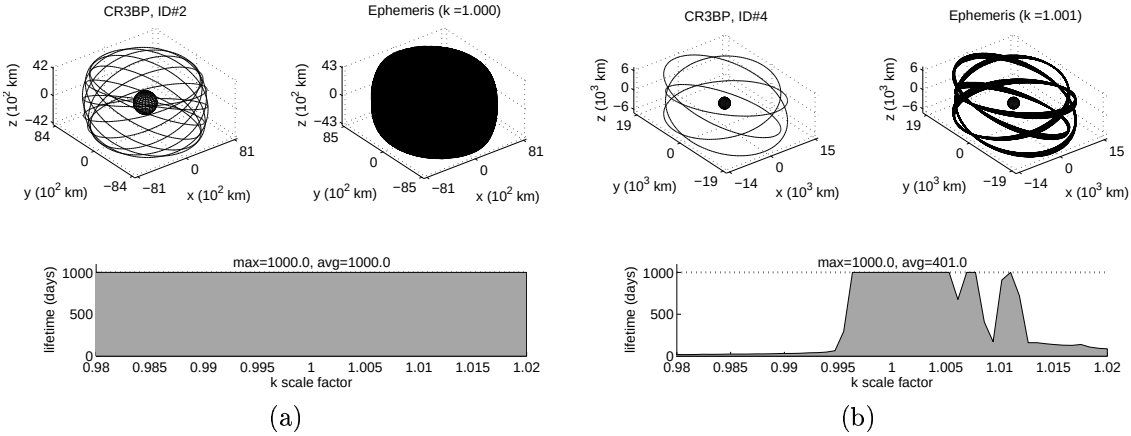

Figure 22: Retrograde solutions near the boundary of the stable DRO region.

the 2:11 resonance family and exists entirely in the large DRO stablitiy region that certainly is intact in the ephemeris. The second case, Fig. 22(b) is near the boundary of the same stablility region much further from Euroapa, and shows long lifetimes for about half of the range of k mappings.

While the stability maps and the linear stability indices show that the halo families do indeed have stable regions in the CRTBP, Figure 23 indicates that this region is too small to combat the perturbing forces introduced with a true ephemeris. It is noted, however, that in the best cases, the trajectories do linger on the order of 10 revolutions or 15 days, much longer than what is typical for a halo orbit near the libration points.

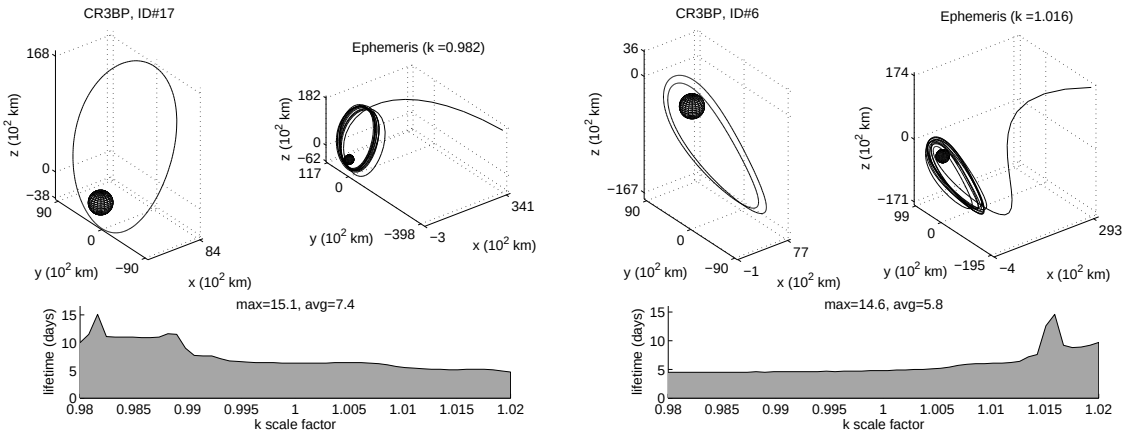

(a) (b)

Figure 23: Example Halo orbits stable in the CRTBP.

Finally, Fig. 24 gives a few examples of some direct orbits. The orbit (a) of that figure is part of the egg-shaped family with resonance 6:17 also shown in Fig. 14. The orbit is generally stable, as indicated by the band of 1000 day lifetimes. The close approach to Europa exacerbates the perturbing effects from the ephemeris and thus many values of k lead to impact. The orbit (b) is part of the 3D egg-shaped family that likely bifurcates vertically from a horizontally bifurcated planar solution of high resonance. Its initial conditions were obtained from the stability region of the stability maps of Fig. 2. The orbits (c) and (d) are also initiated from Fig. 2. These are 3D orbits that are symmetric with respect to x axis and likely bifurcate vertically from a horizontal bifurcation from the simple periodic circular curve. As the orbits (c) and (d) indicate, certain values of k lead to very long lifetimes, but the low close approach tends for most runs to end in impact. Other solutions with higher close approaches exist with with the long lifetimes and because they extent nearly to the libration points, these orbits may have applications for transfer orbits.

Similar to the direct case, several ephemeris runs are also initiated based on speculative regions of interest from the stability maps. An ephemeris run initiated at x=-0.03, z=0.25 from Fig. 17, second row, second column, yields 1000 day lifetimes for roughly half the range of k values, thus substantiating the stability island. This band and the average lifetimes decrease as the energy is decreased and the island grows smaller. The small stability islands in the top right corners of the main stability islands seen in Fig. 18, second row, first column, have also been investigated. The lifetimes show a few peaks of 1000 days but in general, do not show robust stability as indicated by the small radius of the islands on the FLI maps. The more isolated island above the main stability region of Fig. 18, third row and first column, shows a similar behavior, except that the max lifetimes have peaks around 300 days. In this case, similar to the halo region and other strong but small stability regions of the CRTPB, the perturbations associated with the real ephemeris prove too strong, and the islands dissapppear (at various dephts) below the surface of the chaotic sea.

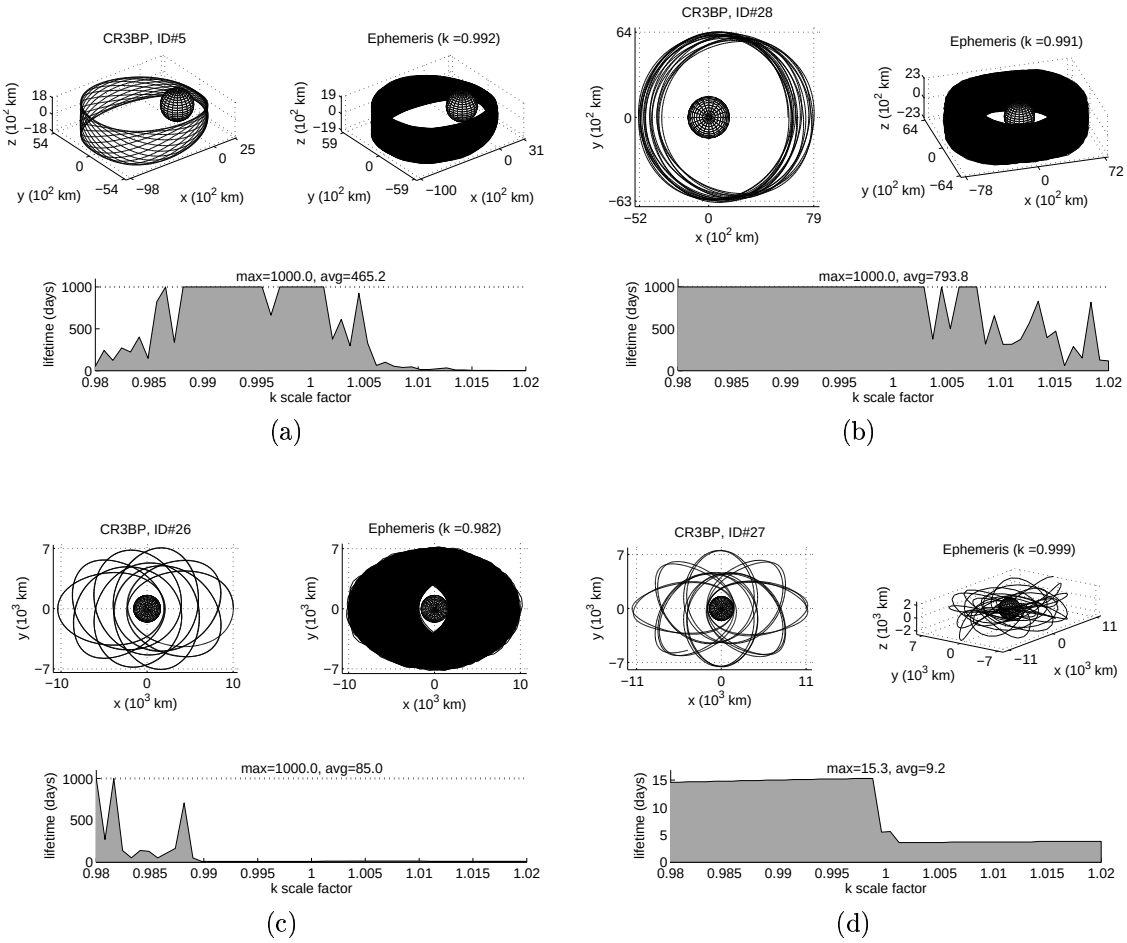

Figure 24: Direct examples.

CONCLUSIONS

A combination of tools arising from dynamical systems theory allows us to determine different regions of long-term stability around Europa that are well suited to locate parking orbits. Further, we described the mutual relations between different regions, and clarified how the different structures —stability regions, periodic orbits— relate to each other.

The computation of periodic orbits of the CRTBP, both in two and three dimensions, provided the basic backbone of the stability regions. The subsequent use of FLI-based stability maps around the periodic orbits of interest, helps in identifying safe regions in three dimensions where to choose nominal orbits robust to small perturbations. The tests performed on a selected set of solutions using a real ephemeris model, showed this procedure as highly reliable.

We only dealt with vertical bifurcations of the main families of planar orbits, paying special attention to the retrograde family, which provides large areas of long-term stability. However, the horizontal bifurcations of the main families will provide new families of planar orbits whose vertical bifurcations could direct to new stability regions. That work is in progress, and we expect to provide new results in a near future.

ACKNOWLEDGEMENTS

Part of this work has been performed at the Jet Propulsion Laboratory , California Institute of Technology, under a contract with the National Aeronautics and Space Administration. Martín Lara acknowledges partial support from the Spanish Government (project numbers ESP2004-04376 and ESP-2005-07107).

APPENDIX: DYNAMICAL MODELS

The restricted three-body problem

We assume that Jupiter and Europa evolve in circular orbits around their mutual center of mass. In a synodic system with the origin at Europa and Jupiter to the left, the equations of motion of the CRTBP are

$$\ddot{x} - 2\dot{y} = \Omega_x, \qquad \ddot{y} + 2\dot{x} = \Omega_y, \qquad \ddot{z} = \Omega_z, \tag{4}$$

where the potential function is

$$\Omega = \frac{1}{2}\left[(x+1-\mu)^2 + y^2\right] + \frac{1-\mu}{\rho} + \frac{\mu}{r} \tag{5}$$

and ρ and r are the distances to Jupiter and Europa respectivelly

$$\rho^2 = (x+1)^2 + y^2 + z^2, \qquad r^2 = x^2 + y^2 + z^2. \tag{6}$$

Equations (4) accept the Jacobi integral

$$\mathcal{J} \equiv 2\Omega(x,y,z) - (\dot{x}^2 + \dot{y}^2 + \dot{z}^2) = C, \tag{7}$$

where C is the Jacobi constant.

Note that we used normalizing units of length and time. In these units $\mu = 2.528 \times 10^{-5}$, and the equatorial radius of Europa is $r_{\mathrm{E}} = 2.334 \times 10^{-3}$. Changing to the baricentric origin is made by simply adding $1-\mu$ to the coordinate x.

Ephemerides model

The ephemeris model is based on three publicly available estimated solutions for the parameters, positions, velocities, and orientations of celestial bodies of interest. The JUP230 [27] solution provides the most recent estimate for the parameters and body states associated with the Jupiter system based on Galileo data. The DE405 [28, 29] solution provides the body states for the barycenters of each of the major planets. The body orientation information is obtained via the `pck00008.tpc` [30] file that is primarily based on the results from the IAU/IAG Working Group on Cartographic Coordinates and Rotational Elements of the Planets and Satellites in 2000 [31]. All three of the necessary files and readers are available from the SPICE [32] information system created at the Jet Propulsion Laboratory. The specific bodies and associated parameters used for all ephemeris propagations in this study are included in Tables 1 and 2.

Initial conditions of some resonant periodic orbits

Tables 3 and 4 of the Appendix provide initial conditions of 88 families of periodic orbits that bifurcate vertically at 44 different resonances. As presented in Fig. 25, these resonances provide a dense set of points covering the part of the retrograde family we are interested in this work. Many other resonances closer to Europa were computed in [4].

Table 1: Active bodies and gravitational parameters

Body	GM (km^3/s^2)	GM source	Position source
Io	5.959916033410404E+03	JUP230	JUP230
Europa	3.202738774922892E+03	JUP230	JUP230
Ganymede	9.887834453334144E+03	JUP230	JUP230
Callisto	7.179289361397270E+03	JUP230	JUP230
Jupiter	1.266865349218008E+08	JUP230	JUP230
Saturn	3.794062976400000E+07	JUP230	DE405
Uranus	5.794548600000000E+06	JUP230	DE405
Neptune	6.836534900000000E+06	JUP230	DE405
Sun	1.327132332402215E+11	JUP230	DE405

Table 2: Non-zero spherical harmonic coefficients for the active bodies

Body	Term	Un-normalized value	Source
Europa	J2	4.355E−04	Ref. [19]
Europa	C22	1.315E−04	Ref. [19]
Jupiter	J2	1.469642900697847E−02	JUP230
Jupiter	J3	−6.436411055625769E−07	JUP230
Jupiter	J4	−5.871402915754995E−04	JUP230
Jupiter	J6	3.425025517100406E−05	JUP230

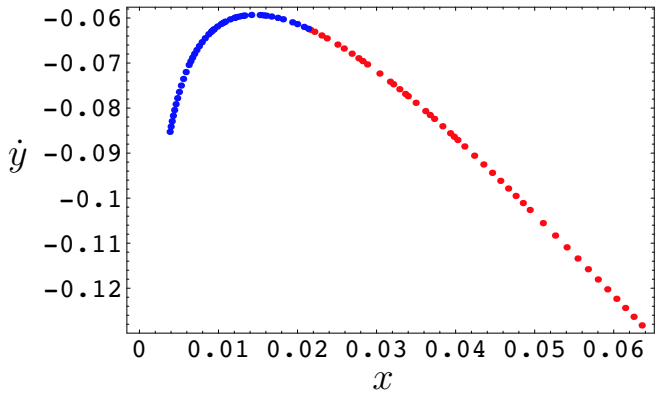

Figure 25: Resonant orbits close to (blue) and further away (red) from Europa.

Table 3: 44 vertical bifurcation resonant orbits of the equatorial retrograde family of the CRTBP close to Europa

d:n	x	$\dot{y}$	T	k_{h}
1:23	0.3826155041228084E−02	−0.8526740864266236E−01	0.2833375384917917E+00	1.916645
1:22	0.3951211985392241E−02	−0.8410826617564759E−01	0.2967692219374928E+00	1.908514
1:21	0.4087028454079570E−02	−0.8291796134798371E−01	0.3115436314871053E+00	1.899142
1:20	0.4235169389432638E−02	−0.8169450285892589E−01	0.3278737803889397E+00	1.888264
1:19	0.4397531720600449E−02	−0.8043572747028210E−01	0.3460205352167187E+00	1.875543
1:18	0.4576439877897677E−02	−0.7913929251393015E−01	0.3663069509926575E+00	1.860539
1:17	0.4774777052176328E−02	−0.7780267586322978E−01	0.3891381319207067E+00	1.842679
1:16	0.4996169162163832E−02	−0.7642319031077169E−01	0.4150292982030582E+00	1.821195
1:15	0.5245248544734603E−02	−0.7499802485045896E−01	0.4446463540446393E+00	1.795050
1:14	0.5528041807889960E−02	−0.7352433578380875E−01	0.4788660651113937E+00	1.762808
1:13	0.5852557764653064E−02	−0.7199943074351844E−01	0.5188680602518417E+00	1.722443
1:12	0.6229711060409965E−02	−0.7042112944944802E−01	0.5662805993161336E+00	1.671029
2:23	0.6442585834317579E−02	−0.6961157610440885E−01	0.5934535710011006E+00	1.639894
1:11	0.6674837113397634E−02	−0.6878847155549984E−01	0.6234216802580490E+00	1.604212
2:21	0.6929498582707031E−02	−0.6795211654087421E−01	0.6566507878093163E+00	1.563067
1:10	0.7210313224874694E−02	−0.6710313814051030E−01	0.6937195968865385E+00	1.515310
2:19	0.7521965203620929E−02	−0.6624264111146694E−01	0.7353572832931125E+00	1.459476
1:09	0.7870414158997231E−02	−0.6537243691588972E−01	0.7824979055137733E+00	1.393679
2:17	0.8263391921073332E−02	−0.6449539928279402E−01	0.8363614496958487E+00	1.315463
1:08	0.8711167909944450E−02	−0.6361603394540601E−01	0.8985789394543692E+00	1.221586
3:23	0.9046852360368484E−02	−0.6303184803246194E−01	0.9457722554469952E+00	1.148212
2:15	0.9227782626247681E−02	−0.6274142865140307E−01	0.9713942419179452E+00	1.107700
3:22	0.9418498005530136E−02	−0.6245274019643721E−01	0.9985369409854700E+00	1.064325
1:07	0.9833151434219369E−02	−0.6188292069217829E−01	0.1058008159074479E+01	0.967878
3:20	0.1030009028276802E−01	−0.6132830864874999E−01	0.1125684848630590E+01	0.856311
2:13	0.1055692893154534E−01	−0.6105923085764407E−01	0.1163209279870955E+01	0.793876
3:19	0.1083190541690132E−01	−0.6079742485591100E−01	0.1203605734857834E+01	0.726380
1:06	0.1144636611350280E−01	−0.6030294133108111E−01	0.1294651484142512E+01	0.573927
4:23	0.1197685684557419E−01	−0.5996743109372164E−01	0.1374046774174339E+01	0.441589
3:17	0.1216990502454047E−01	−0.5986458802845467E−01	0.1403106282203926E+01	0.393497
2:11	0.1258484318004971E−01	−0.5967592114004498E−01	0.1465846672906467E+01	0.290587
3:16	0.1304489475478843E−01	−0.5951522777183572E−01	0.1535822527217163E+01	0.177707
4:21	0.1329500392154116E−01	−0.5944790706816894E−01	0.1574033119153793E+01	0.117092
1:05	0.1414754818442209E−01	−0.5931577338986633E−01	0.1705062259033207E+01	−0.084105
4:19	0.1521699626514246E−01	−0.5934037032234122E−01	0.1870811898885309E+01	−0.320890
3:14	0.1564580518845134E−01	−0.5940322748867374E−01	0.1937594402971556E+01	−0.409910
5:23	0.1602577653009806E−01	−0.5948215937268645E−01	0.1996883313977625E+01	−0.485649
2:09	0.1667806482778222E−01	−0.5966543432801284E−01	0.2098836665591457E+01	−0.608402
5:22	0.1747753426456767E−01	−0.5996640285399415E−01	0.2223934174440752E+01	−0.745756
3:13	0.1814851772097931E−01	−0.6027867857993052E−01	0.2328886035791364E+01	−0.849599
4:17	0.1933048745510534E−01	−0.6094887675807979E−01	0.2513222774023195E+01	−1.007126
9:38	0.1994693483076238E−01	−0.6135419221344066E−01	0.2608872657482850E+01	−1.076733
5:21	0.2079970106729542E−01	−0.6197264163328550E−01	0.2740373013495280E+01	−1.159496
41:172	0.2133267537429230E−01	−0.6239114754380821E−01	0.2821960235195845E+01	−1.203622

Table 4: 44 vertical bifurcation resonant orbits of the equatorial retrograde family of the CRTBP far away from Europa

d:n	x	$\dot{y}$	T	k_{h}
1:23	0.6353941003776735E−01	−0.1282527195536677E+00	0.5886109062321278E+01	0.979606
1:22	0.6250799648758544E−01	−0.1263506882327820E+00	0.5867551814766511E+01	0.936367
1:21	0.6144038042188015E−01	−0.1243862237302853E+00	0.5847166767231673E+01	0.889348
1:20	0.6033316664960482E−01	−0.1223539227755164E+00	0.5824668659952298E+01	0.838041
1:19	0.5918241207212686E−01	−0.1202475789617227E+00	0.5799709296264242E+01	0.781848
1:18	0.5798349459948331E−01	−0.1180600054901806E+00	0.5771859058725420E+01	0.720057
1:17	0.5673093888800879E−01	−0.1157828038360492E+00	0.5740581452420173E+01	0.651815
1:16	0.5541818013596126E−01	−0.1134060564443594E+00	0.5705197370513562E+01	0.576099
1:15	0.5403723669442891E−01	−0.1109179100941403E+00	0.5664833835022133E+01	0.491669
1:14	0.5257824436860801E−01	−0.1083039974389727E+00	0.5618348618540506E+01	0.397016
1:13	0.5102877343660671E−01	−0.1055466109709242E+00	0.5564216150606297E+01	0.290300
1:12	0.4937278975817452E−01	−0.1026234829019499E+00	0.5500348835196873E+01	0.169268
2:23	0.4849847231578456E−01	−0.1010911183208486E+00	0.5463890424275696E+01	0.102548
1:11	0.4758900261213762E−01	−0.9950590666362791E−01	0.5423805492824410E+01	0.031180
2:21	0.4664044624656298E−01	−0.9786275744273229E−01	0.5379511649998888E+01	−0.045265
1:10	0.4564808727934198E−01	−0.9615568986027044E−01	0.5330290902841109E+01	−0.127248
2:19	0.4460619179881776E−01	−0.9437758897042788E−01	0.5275246210224154E+01	−0.215258
1:09	0.4350767035328467E−01	−0.9251986487884503E−01	0.5213239387063441E+01	−0.309796
2:17	0.4234358048347177E−01	−0.9057196144060517E−01	0.5142799767827626E+01	−0.411350
1:08	0.4110236517985263E−01	−0.8852062094221445E−01	0.5061985114906921E+01	−0.520346
3:23	0.4022465127732229E−01	−0.8708735404640827E−01	0.5001081789255903E+01	−0.597292
2:15	0.3976863140197200E−01	−0.8634873145297553E−01	0.4968160512789386E+01	−0.637063
3:22	0.3930004068751295E−01	−0.8559424469954729E−01	0.4933396357147299E+01	−0.677693
1:07	0.3832107250811104E−01	−0.8403341105503616E−01	0.4857627165556660E+01	−0.761473
3:20	0.3727806128222297E−01	−0.8239488070964222E−01	0.4772077094127238E+01	−0.848416
2:13	0.3672865478619085E−01	−0.8154257073309804E−01	0.4724952716492553E+01	−0.892950
3:19	0.3615802798079715E−01	−0.8066564828086240E−01	0.4674469719248956E+01	−0.938088
1:06	0.3494285439023597E−01	−0.7882807035097809E−01	0.4561636930384047E+01	−1.029699
4:23	0.3395345680098102E−01	−0.7736402285143601E−01	0.4464314754503994E+01	−1.098887
3:17	0.3360582717701666E−01	−0.7685689805782549E−01	0.4428943829989498E+01	−1.121877
2:11	0.3287929526380078E−01	−0.7580986301805218E−01	0.4353033836336723E+01	−1.167484
3:16	0.3210440444511792E−01	−0.7471313833378794E−01	0.4269105948212905E+01	−1.212195
4:21	0.3169566010781211E−01	−0.7414333571927938E−01	0.4223604145457339E+01	−1.234023
1:05	0.3036237982477276E−01	−0.7232907473034086E−01	0.4069323294120554E+01	−1.296036
4:19	0.2880506661070283E−01	−0.7030301573492564E−01	0.3878020147298908E+01	−1.348824
3:14	0.2821209263677290E−01	−0.6956017779018046E−01	0.3802149426431286E+01	−1.362809
5:23	0.2770024809963163E−01	−0.6893249162873222E−01	0.3735368228733427E+01	−1.371975
2:09	0.2684926734310894E−01	−0.6791797246249998E−01	0.3621788175578199E+01	−1.380937
5:22	0.2585007529673770E−01	−0.6677581101439256E−01	0.3484572346987732E+01	−1.380780
3:13	0.2504538985568889E−01	−0.6589709230384662E−01	0.3371253241367818E+01	−1.371594
4:17	0.2369569281198253E−01	−0.6451235735145495E−01	0.3176115797553956E+01	−1.336141
9:38	0.2302319274726586E−01	−0.6386723923684007E−01	0.3076778119343246E+01	−1.308181
5:21	0.2212553399144233E−01	−0.6305635689305078E−01	0.2942295105652748E+01	−1.259089
41:172	0.2158269930150112E−01	−0.6259553900765756E−01	0.2860049250900922E+01	−1.222396

References

[1] Villac, B.F., Lara, M., "Stability maps, Global Dynamics and Transfers", paper AAS 05-378 2005 AAS/AIAA Astrodynamics Specialists Conference, Lake Tahoe, California.

[2] Johannesen, J.R., and D'Amario, L.A., "Europa Orbiter Mission Trajectory Design (AAS 99-360)," *Astrodynamics 1999*, edited by K.C. Howell et al., Vol. 103, Advances in the Astronautical Sciences, Univelt, San Diego, California, 1999, pp. 895–908.

[3] Scheeres, D.J., Guman, M.D., and Villac, B.F., "Stability Analysis of Planetary Satellite Orbiters: Application to the Europa Orbiter," *Journal of Guidance, Control, and Dynamics*, Vol. 24, No. 4, 2001, pp. 778–787.

[4] Lara, M., and San-Juan, J.F., "Dynamic Behavior of an Orbiter Around Europa." *Journal of Guidance, Control and Dynamics*, Vol. 28, No. 2, 2005, pp. 291–297.

[5] San-Juan, J.F., Lara, M., and Ferrer, S., "Phase space structure around planetary satellites," paper AIAA 2004-4863, presented at AIAA/AAS Astrodynamics Specialist Conference and Exibit. Providence, RI, August 2004.

[6] Paskowitz, M.E., and Scheeres, D.J., "Orbit Mechanics About Planetary Satellites Including Higher Order Gravity Fields," paper AAS 2005-190, presented at the 2005 Space Flight Mechanics Meeting, Copper Mountain, Colorado, January 2005.

[7] Whiffen, G., "A Preliminary Investigation of the Jupiter Icy Moon Orbiter", AAS paper 03-354, presented at the 2003 AAS/AIAA Astrodynamics Specialists Conference, Big Sky, Montana.

[8] Lam, T., Whiffen, G.J., "Exploration of Distant Retrograde Orbits around Europa," paper AAS 05-110, presented at the 15^{th} Spaceflight Mechanics Meetings, Copper Mountain, Colorado, January 2005.

[9] Villac, B.F., Aiello, J., "Mapping Long-term stability regions using the Fast Lyapunov Indicator", paper AAS 05-188, presented at the 15^{th} Spaceflight Mechanics Meetings, Copper Mountain, Colorado, January 2005.

[10] Froeschle, C., Lega, E., "Fast Lyapunov Inidcators. Application to Asteroidal Motion.", *Celestial Mechanics and Dynamical Astronomy*, Vol. 67, pp. 41–62, 1997.

[11] Marzari, F., Scholl, H., "On the instability of Jupiter's Trojans", *Icarus*, Vol. 159, pp. 328-338, 2002.

[12] Szebehely, V., *Theory of Orbits — The Restricted Problem of Three Bodies,* Academic Press, New York, 1967.

[13] Wiggins, S. *Introduction to applied nonlinear dynamical systems and chaos*, Texts in applied mathematics, Vol. 2, Springer-Verlag, 1990.

[14] Broucke, R., "Stability of Periodic Orbits in the Elliptic Restricted Three-Body Problem," *AIAA Journal*, Vol. 7, No. 6, 1969, pp. 1003–1009.

[15] Hénon, M., "Vertical Stability of Periodic Orbits in the Restricted Problem.II. Hill's case", *Astronomy and Astrophysics*, Vol. 30, 1974, pp. 317–321.

[16] Hénon, M., "Exploration Numérique du Problème Restreint. II. Masses égales, stabilité des orbites périodiques," *Ann. and Astrophys.*, Vol. 28, No. 2, 1965, pp. 992–1007.

[17] Robin, I.A., and Markellos, V.V., "Numerical Determination of Three-dimensional Periodic Orbits Generated from Vertical Self-resonant Orbits," *Celestial Mechanics*, Vol. 21, 1980, pp. 395–434.

[18] Davoust, E., and Broucke, R., "A Manifold of Periodic Orbits in the Planar General Three-body Problem with Equal Masses," *Astronomy and Astrophysics,* Vol. 112, 1982, pp. 305–320.

[19] *Jupiter, The Planet, Satellites, and Magnetosphere*, edited by F. Bagenal, T. Dowling, W. McKinnon, Cambridge Planetary Society, Cambridge, United Kingdom, 2004, p. 285.

[20] Lara, M., and Scheeres, D.J., "Stability bounds for three-dimensional motion close to asteroids." *The Journal of the Astronautical Sciences*, Vol. 50, No. 4, 2002, pp. 389–409.

[21] Hénon, M., "Numerical exploration of the restricted problem. VI. Hill's Case: non-periodic orbits", *Astronomy & Astrophysics* Vol., 9, 1970, pp. 24–36.

[22] Darwin, G.H., "Periodic Orbits", *Acta Mathematica*, Vol. 21, 1897, p. 99; also "Scientific Papers", Vol. 4, p. 140. Cambridge University Press, London and New York, 1911.

[23] Broucke, R.A., *Periodic Orbits in the Restricted Three-Body Problem With Earth-Moon Masses*, NASA-JPL TR 32-1168, February 1968, p. 71 (100 pages).

[24] Hénon, M., "New Families of Periodic Orbits in Hill's Problem of Three Bodies", *Celestial Mechanics and Dynamical Astronomy*, Vol. 85, Issue 3, 2003, pp. 223–246.

[25] Simo, Stuchhi,"Central stable/unstable manifolds and the destruction of KAM tori in the planar Hill problem", *Physica D*, Vol. 140, No. 1-2, pp. 1-32, 2000.

[26] Rusell, R.P., "Global Search for Planar and Three-Dimensional Periodic Orbits near Europa", AAS paper 05-290, presented at the same conference.

[27] URL: `ftp://naif.jpl.nasa.gov/pub/naif/generic_kernels/spk/satellites/jup230.bsp` [cited 22 June 2005].

[28] URL: `ftp://naif.jpl.nasa.gov/pub/naif/generic_kernels/spk/planets/de405_2000-2050.bsp` [cited 22 June 2005].

[29] Standish, E. M., *JPL Planetary and Lunar Ephemerides*, CD-ROM, Willman-Bell Inc., Richmond, VA, 1997.

[30] URL: `ftp://naif.jpl.nasa.gov/pub/naif/generic_kernels/pck/pck00008.tpc` [cited 22 June 2005].

[31] Seidelmann, P.K., Abalakin, V.K., Bursa, M., Davies, M.E., Bergh, C. de, Lieske, J.H., Oberst, J., Simon, J.L., Standish, E.M., Stooke, P., and Thomas, P.C., "Report of the IAU/IAG Working Group on Cartographic Coordinates and Rotational Elements of the Planets and Satellites: 2000," *Celestial Mechanics and Dynamical Astronomy*, Vol. 82, Issue 1, 2002, pp. 83–111.

[32] URL: `http://naif.jpl.nasa.gov/naif/spiceconcept.html` [cited 22 June 2005].